Fluvial connectivity of a deep-seated landslide to upstream tree harvests

Jeffrey Keck

A report prepared in partial fulfillment of
the requirements for the degree of

Master of Science
Earth and Space Sciences: Applied Geosciences

University of Washington

March, 2017

Project mentor:
Brian Collins

Internship coordinator:
Kathy Troost

Reading committee:
Brian Collins
Alison Duvall
Casey Hanell

MESSAGe Technical Report Number: 048

Abstract

Channel wall scour may have debuttressed a deep-seated landslide located in a small, mountainous drainage in the Clearwater River Watershed in the western Olympic Mountains, Washington State. Debris flows and high peak flows, both of which can cause channel wall scour, may have been caused by upstream tree harvests. Through examination of stream flow, debris flow and precipitation records relative to the tree harvest and deep-seated landslide activity records, tree harvest effects on the deep-seated landslide are clarified.

Following harvest on the landslide, evidence of deep seated landslide activity is undetectable until the trees upstream of the landslide are harvested. In total, three periods of landslide activity are observed. High stream flow (a 25-year event) coincides with one period of activity; however, the magnitude of flow events larger than a 1.1-year event are unaffected by tree harvests. High precipitation and snow melt (water input) events coincide with two of the landslide events but at the time of landslide activity, evapotranspiraiton rates of the plantation trees may have been nearly equal to that of the original forest. In contrast, debris flows, which coincide with all periods of deep-seated landslide activity, dramatically increase following harvest in the headwaters despite below average annual maximum 1-day precipitation and no change in annual maximum 30-day precipitation. Tree harvests in the headwaters of the watershed appear to have caused the increase in debris flow frequency which in turn triggered landslide activity.

Table of contents

List of Tables

Acknowledgments

Teodora Minkova, Warren Devine, Ellis Cropper and Rebekah Korenowsky installed and managed the gage at the outlet of East Fork Kunamaskt Creek. I am greatly indebted to them for letting me use the discharge data in this project.

Early on, Kathy Troost, Juliet Crider, Alison Duvall and David Montgomery provided helpful advice that set the direction of the project. Casey Hanell and Orion George also helped direct the project and provided valuable training in the field.

Throughout the project, Brian Collins gave helpful feedback and guidance as I tried to synthesize multiple field and modeling investigations into one report. Erkan Istanbullouglu provided the training and MATLAB scripts needed to implement the snow and flow modeling techniques used in this study.

Finally, the dendrogeomorphology techniques applied in this study are methods I learned with William Wright and coworkers at Sinotech Engineering Consultants, Inc. Without the training from William or support from Sinotech, I would not have been able to date periods of landslide movement.

1. Introduction

Public awareness of deep-seated landslide hazards is increasing in the State of Washington. That awareness is in part due to the availability of high resolution topography data (PSLC, 2016) that has revealed the locations of numerous unmapped deep-seated landslides. It is also due to unchecked urban-sprawl and development of wildlands near Seattle (Robinson et al., 2005) that contain deep-seated landslide prone terrain. Moreover, the 2014 Oso landslide disaster (GEER, 2014) further increased awareness of the consequences of building homes near deep-seated landslides and highlighted the possible role of tree harvests as a cause of deep-seated landslides.

Few studies have specifically documented timber harvest effects on the stability of deep-seated landslides and our understanding of the processes by which removing trees might destabilize an existing deep-seated landslide or trigger a new deep-seated landslide is limited. Swanston and Swanson (1977) detailed deep-seated landslide processes in Oregon following complete removal of the trees in a basin but no inference on how harvest affected the slides were made. In a case study of a deep-seated landslide in Oregon, Pyles et al. (1987) reported that activity was triggered by a rise in pore water pressure of only 1.4 ft in the shear zone of the deep seated landslide but that because the landslide was well-drained, soil water increases caused by timber harvest were not likely to cause large movement.

Miller (1995) examined the effect of timber harvest on a glacial, deep-seated landslide located on the Oso landslide using Bishop's Simplified Method of Slices to estimate landslide stability for several different soil moisture and landslide topography conditions. In that study, landslide stability was found to be very sensitive to increases in pore water pressure and changes in soil water caused by tree harvests in the contributing area to the landslide. Miller and Sias (1998) again assessed timber harvest affects on the Oso landslide by coupling the same slope stability model with a simplified ground water model and assumptions of the subsurface conditions. In that study, they found that stability of the Oso landslide was dependent on five-year antecedent moisture and that changes in ground water that resulted from timber harvest might not affect the landslide for several years.

In contrast to deep-seated landslides, timber harvest effects on shallow landslides and the processes that control shallow landslide occurrence such as soil water and root cohesion are well documented. Past studies have shown that; (1) Timber harvesting accelerates erosion rates by increasing the frequency of landslides (Sidle, 1992, Montgomery et al., 2000, Guthrie, 2002, Wolter et al., 2010); (2) Roads constructed to access the timber are a major source of sediment and can destabilize hillslopes by oversteepening and concentrating water onto the landscape (Guthrie, 2002, Wemple et al., 2001); (3) Shortly following harvest, effective cohesion from tree roots is reduced

(Skaugset 1997) but if replanted immediately following the harvest, effective cohesion may be regained after 15 to 25 years (Schmidt et al., 2001); (4) Rainfall intensity on bare soil and resultant pore water pressures are higher than that under a mature tree canopy (Keim and Skaugset, 2003, Johnson et al., 2007).

This study adds to the limited body of knowledge on how timber harvests affect deep-seated landslides. The focus of the study is an extremely slow (Cruden and Varnes, 1996), bedrock deep-seated landslide that is at least several hundred years old and presently constricts a small tributary of the Clearwater River in the western Olympic Mountains, Washington State. Trees growing on the landslide and headwaters upstream of the landslide were harvested and re-planted in the late 20th century. This study tests the hypothesis that harvests reactivated the deep-seated landslide by triggering debris flows or high peak flows that subsequently scoured and debuttressed the toe of the landslide.

To test this hypothesis, this study: (1) identifies what processes triggered landslide activity and (2) assesses how vegetation removal affected those processes. Three processes are considered as possible triggers: elevated pore water pressures that result from high rainfall and snowmelt (water input), peak flows that scour and debuttress the toe of the landslide and debris flows that scour and debuttress the toe of the landslide.

To demonstrate that each process is a possible landslide trigger, a sensitivity analysis of slope stability to changes in pore water pressures and scour width into the toe is conducted. To determine what years each process may have triggered activity, the timing of each process is compared to the timing of deep-seated landslide activity; years of landslide activity that coincide with years of any certain process are inferred to indicate that the process may be a trigger. To assess the effect of vegetation removal on water input and stream flow, a snow ablation and melt model and a lumped hydrologic model calibrated to three years of flow observations are used. Vegetation removal effects on debris flows are determined by comparing precipitation and harvest records to the timing of debris flows.

2. Description of study location

2.1 Tectonic and geomorphic setting

The deep-seated landslide is located in the upper reaches of East Fork Kunamaskt Creek, a tributary of the Clearwater River Watershed on the west side of the Olympic Mountains (Figure 1). The Olympic Mountains define the northern part of a forearc-high that is currently uplifting between the Cascadia Subduction Zone and the North American Plate. The forearc high includes the Coast Range of Oregon and Washington and extends from the Klamath Mountains of Northern California to the

Insular Mountains of Vancouver Island (Orr and Orr, 1996). Elevations in the forearc-high range from just a few hundred to over 2,400 meters. The highest peaks and most incised channels are found in the Olympic Mountains.

Most of the Cascadia Forearc-High is underlain by the Coast Range Terrain (Batt et al, 2001). The Coast Range Terrain is one of many terrains that accreted along the northwest coast of the North American Plate as it drifted northwest and west after splitting from Pangea (Orr and Orr, 1996). Presently, the Cascadia Wedge, which is the most recently accreted terrain to form off of the northwest coast of North America, is building to the west of and underneath the Coast Range Terrain. Accommodation of the accreted terrain onto the continent is occurring by both the continued westward buildup of new material as well as via storage of material underneath the Coast Range Terrain. As a consequence of that storage, both deformation of the wedge material and rapid uplift of the Coast Range Terrain is occurring (Brandon et al, 1998). Uplifted rock is fractured, folded, sheared and weak.

Near the Olympic Mountains, the Cascadia Subduction Zone is 10 km shallower than the subduction zone at other areas of the convergent margin. Because less accommodation space is available to store the accreted materials, uplift rates are as high as 1.2 to 3.2 m/ky (Pazzaglia and Brandon, 2001) and long term uplift has averaged 0.3 m/ky (Brandon et al., 1998). In response to the rapid uplift, erosion, via hillslope, fluvial and glacial processes, has also been rapid; since the late Miocene, erosion rates have ranged from 0.3 to 0.8 m/ky and averaged 0.32 m/ky during modern times (Pazzaglia and Brandon, 2001).

Erosion has roughly equaled uplift rates to maintain steady-state topography for the last 14 Ma (Brandon et al., 1998) and over time, accumulated erosion has exceeded the depth of the Coast Range Terrain so that in that in the Olympic Mountains, the Cascadia Wedge is exposed subaerially. This isolated exposure of the Cascadia Wedge on the Olympic Peninsula is known as the Olympic Subduction Complex (OSC). The Clearwater River Watershed and East Fork Kunamaskt Creek are underlain by the OSC.

2.2 East Fork Kunamaskt Creek

East Fork Kunamakst Creek is located beyond the extent of Quaternary continental and alpine glaciers and erosion rates during the last 2.6 Ma have been controlled by fluvial and hillslope processes. Ancient, consolidated debris flow deposits form a large terrace at a confluence in the lower half of the basin (Figure 1). Smaller debris flow deposits are located on strath terraces adjacent to the channel and more recent deposits form terraces in the channel. High fall and winter precipitation that annually

exceeds 3m/yr (WRCC, 2016) have maintained incision rates ranging from 0.1 m/ky to 0.9 m/ky. (Pazzaglia and Brandon, 2001).

Slope in the basin varies from 25 to 75 degrees on hillslopes and 5 to 15 degrees on the ancient debris flow terrace. Elevation ranges from 260 to 850 meters. Most of the basin is in the Rain-on-Snow Zone (WA DNR, 2016) and rain-on-snow water input (rain plus snowmelt) does affect the timing of water released into the basin.

East Fork Kunamask Creek is underlain by the Western Olympic Lithic Assemblage which consists of indurated multistory sandstones divided by laminated sandstone and siltstone couplets. The closest active fault (active during the Quaternary) is Calawah fault located 45 km north of the basin. East-west and north-south trending inactive faults are located within 15 km of the basin (Czajkowski and Bowman, 2014).

Throughout the basin, slickenslides, fault gauge, folded beds and chaotic, densily spaced joints are visible in bedrock exposed in channel walls and road cut-banks. In the lower reaches of the basin, bedrock strikes to the northwest and dips steeply to the north and consists of thin to medium bedded fine grained sandstone and siltstone as well as massive beds of fractured, grey, medium grained sandstone. In the upper reaches of the basin, beds strike more westerly and dip steeply to the south and consist of densely fractured siltstone and sandstone. Previously mapped bedrock attitudes(Gerstel and Lingley, 2000) and new measurements from this study are shown in Figure 1.

A vertical change in ridge topography that coincides with the location of a knick point in East Fork Kunamaskt Creek and two bedrock, deep-seated landslides (Figure 1) may be evidence of a possible northwest-southeast trending fault; however, there is little topographic evidence of the fault outside of the basin. The lack of continuous topographic evidence suggests that any past uplift has since been eroded and that the possible fault may be inactive. Nonetheless, from downstream to upstream along East Fork Kunamaskt Creek, towards the possible fault, joint spacing and persistence increases and rock strength, inferred from the number of hammer blows needed to crack the rock, decreases. (Figure 1)

2.3 The deep-seated landslide

Over a 25 year period, two thirds of the original forest in the East Fork Kunamaskt Creek was gradually logged and re-planted as a tree farm. Logging and re-planting occurred on the landslide in 1981 and on most of the area upstream of the landslide around 1990. At the landslide, large (0.75 to 1.0 m diameter) stumps from the trees of the original forest still cover the crown, main scarp, head, body and toe of the deep-seated landslide. The toe of the deep-seated landslide constricts the channel at the base of the landslide (Figure 2 and 3).

Channel slope adjacent to the landslide toe ranges between 15 to 25% and includes cascade to colluvial channel morphologies (Figure 1). Over the entire length of East Fork Kunamaskt Creek, channel morphology varies from pool-riffle to hollow. Debris flows commonly initiate in colluvial and hollow channel reaches and are a dominant sediment transport and scour mechanism in cascade channels (Montgomery and Buffington, 1997, Benda et al, 1998). Because the toe of the landslide constricts the debris flow-scour reach of the stream, it is susceptible to scour caused debutressing.

In the field, there are mulitple lines of evidence of recent debris flow activity at the toe of the landslide. The current channel has incised into 0.5 to 1 meter deep unsorted cobble and gravel terrace deposits. The walls of the channel adjacent to the landslide are scoured up to a height of 2 to 3 meters above the channel bed. Both the terrace deposits and the scoured channel walls are covered in 5 to 20 year old alders (Figure 3).

The depressed topography of the head of the landslide and bulging body lower in the slope suggest that landslide movement towards the channel is rotational and deep (surface of rupture is below rooting depth of trees); however the presence of large stumps over much of the landslide indicates that movement is extremely slow and that the body has remained on the hillslope in roughly the same position for at least the age of the original forest (several hundred years). Nonetheless, tension cracks, shallow landslide scars, tilted trees and tilted stumps on the right lateral margin and toe indicate that some parts of the landslide are active enough to disturb the surface vegetation.

Bedrock in the channel near the possible fault and at the toe of the landslide consists of massive (5 to 10 meters thick) beds of siltstone interspaced by occasional 50 cm thick beds of coarse grained sandstone. The siltstone and sandstone are highly indurated, but densely fractured and sheared. The siltstone requires only one hammer blow to fracture while the thin, occasional beds of sandstone require multiple hits. The siltstone and sandstone beds dip steeply to the south, perpendicular to the direction of landslide motion.

Figure 1. East Fork Kunamaskt Creek location and geomorphology. Landslide location relative to channel morphology is shown at bottom of figure.

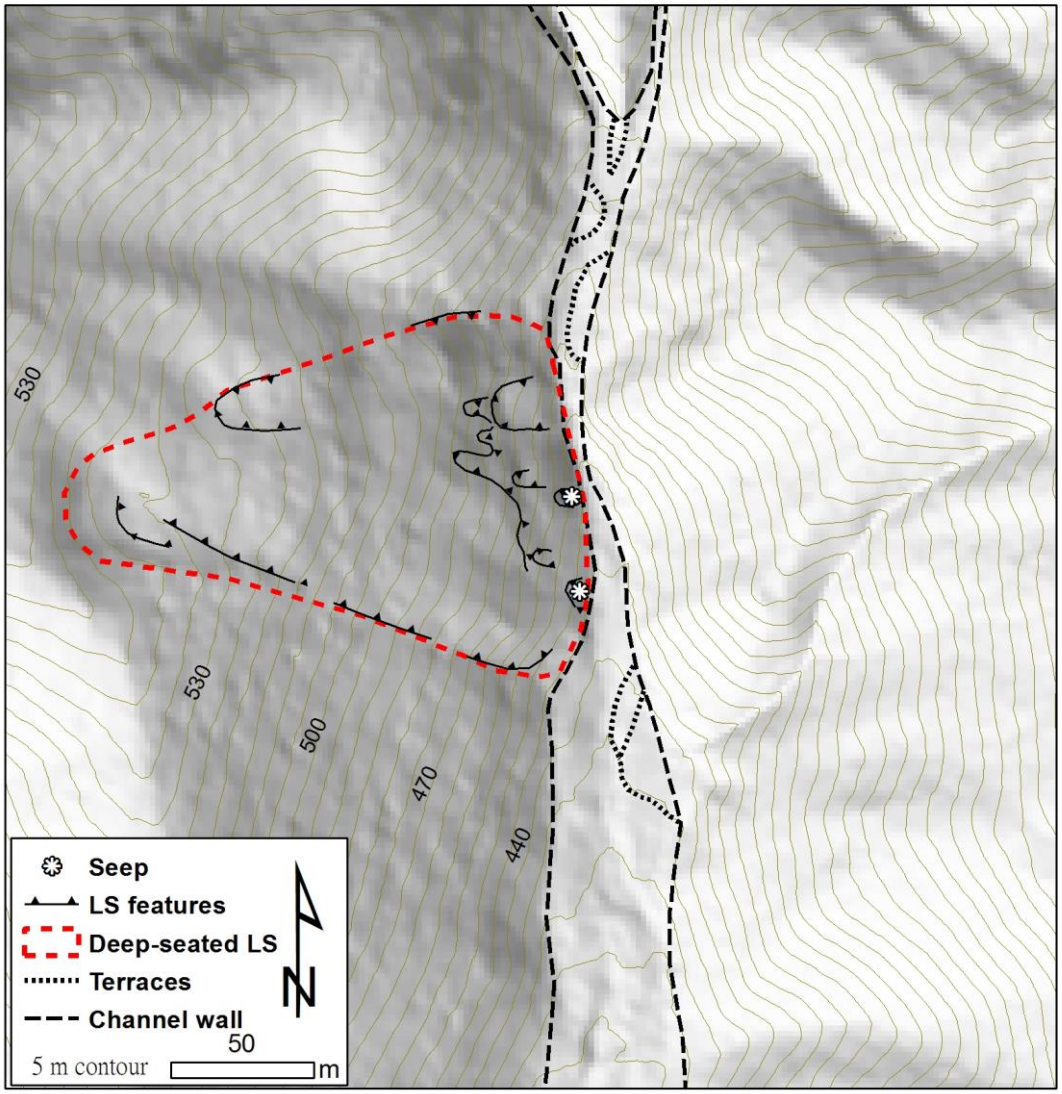

Figure 2. Constricted stream channel at toe of landslide

Figure 3. Looking downstream at the channel adjacent to landslide toe. Right channel wall has been scoured up to 3 meters above the channel bed. Young alders are growing on the channel bed and channel walls.

3. Methods

3.1 Approach

Given the tectonic forces that are controlling uplift and erosion on the Olympic Peninsula, it's hard to imagine how relatively brief, anthropogenic changes in surface vegetation could have had an effect on the landscape. Nonetheless, changes in vegetation are known to alter stream flow and shallow landslide processes and at East Fork Kunmaskt Creek, it is hypothesized that changes in these processes may have affected a deep-seated landslide. Specifically, it is hypothesized that tree harvests in the headwaters of the basin reduced evapotranspiration and root cohesion in hollow and colluvial reaches of the channel which in turn caused an increase in the frequency of floods and debris flows that flowed past, scoured and debuttressed the toe of the deep-seated landslide.

To test this hypothesis, this study: (1) identifies what processes trigger movement of the deep-seated landslide and; (2) assesses how vegetation removal affects those processes. Three processes are considered as potential deep-seated landslide triggers: floods (peak flows) that scour the toe of the landslide, debris flows that scour the toe of the landslide and high water input (rainfall plus snowmelt) that raises pore water pressure in the landslide. To understand how each process might affect landslide stability, a sensitivity analysis of slope stability relative to changes in pore water pressures (water input) and scour width into the toe (debris flows and floods) is conducted. Also, the timing of each process is compared to the timing of deep-seated

landslide activity and the timing of tree harvests. Any years in which a process coincides with deep-seated landslide activity is inferred to indicate that the process may be a landslide trigger.

Because the landslide is located in a remote region, direct observation and record keeping of landslide and debris flow activity are non-existent. Moreover, flow records at the outlet of the basin exist only for the last three years and there are no water input records at the landslide. Therefore, landslide activity, debris flow, water input and flood records are determined indirectly using the following techniques: (1) a detailed dendrogeomorphic survey is used to pinpoint years of deep seated landslide activity; (2) the debris flow record is reconstructed from air photos and a survey of the ages of trees growing in the channel near the landslide toe; (3) water input is computed using a snow accumulation and ablation model that is forced using precipitation and temperature data extrapolated to the basin from a nearby observation station and; (4) flow records are estimated using a lumped hydrologic model that is forced using water input and temperature and calibrated to the three years of flow observations..

To determine harvest effects on water input and peak flows, two extreme vegetation conditions are modeled: fully forested conditions and fully harvested conditions. Fully forested means 100 percent of the basin area is perpetually covered by mature trees. Fully harvested means 100 percent of the basin is perpetually bare except for trace amounts of grass and brush. Because the actual harvests in East Fork Kunamaskt Creek were promptly replanted, the harvest caused changes in water input and peak flows determined in this study are only representative of conditions that existed shortly after harvest.

3.2 Dendrogeomorphic survey

In this study, years of deep seated landslide activity are determined from a dendrogeomorphic survey of the landslide. Dendrogeomorpholgy is a sub-discipline of dendrochronology that uses patterns in the annual rings of a tree to date past geomorphic events (Alestalo, 1971, Fritts, 1976). In this application of dendrogeomorphology, deep-seated landslide activity is inferred from growth disturbances, or sudden changes in the width of the annual rings, in trees that were planted on the landslide after harvest of the original forest in 1981. Because a tree may need to be 10 years old before growth disturbances are discernible from highly variable growth associated with the early life of a tree (Stoffel et al., 2010), only 25 to 30 years of the tree growth could be used to reliably detect landslide movement. Consequently, comparisons of the deep-seated landslide record derived from the dendrogeomorphic survey with water input, debris flows and peak flow records are

limited to 1991 to 2016.

To help ensure that the growth of trees used in the dendrogeomorphic survey are affected by past landslide movement, only parts of the landslide where surface disturbance is greatest are selected for sampling. Surface disturbance is considered greatest where tension cracks, shallow landslide scars and tilted trees are most prevalent. Four general locations are targeted for sampling: (1) where the surface of rupture intersects the hillslope surface along the right lateral margin; (2) the junction of the right edge of the landslide toe and the adjacent hillslope; (3) adjacent to or on shallow landslides occurring on the landslide toe and; (4) along the edge of a depressed area on the left lateral margin of the landslide.

Because slope movement is only one of many factors that can disrupt tree growth (Stoffel et al., 2010), trees that showed signs of other sources of disturbance are excluded from the sample group. In particular, three sources of disturbance other than the landslide are avoided: (1) trees damaged by bears; (2) trees that have more than one top; (3) trees that are growing on unstable wood surfaces such as old stumps or logs. Wind can affect a tree regardless of tree location and is a possible source of disturbance in all sampled trees in this study. Methods for detecting wind disturbance are detailed below.

Once a tree is selected for sampling, four radius cores are extracted and converted to a ring series following methods detailed in Keck et al. (2014). A total of 47 plantation trees are sampled from the landslide. A control sample group is created from an additional four plantation trees growing on the ridge adjacent to but unaffected by the landslide. The landslide sample group consists of four tree species, including: *Pseudotsuga menziesii* (Douglas Fir), *Tsuga heterophylla* (Western Hemlock), *Abies amabilis* (Pacific Silver Fir) and *Thuja plicata* (Western Red Cedar). The control group has only two species: *Pseudotsuga menziesii* and *Tsuga heterophylla*. For each tree, tree species, tilt direction and the direction of each core is noted. Tree location relative to the landslide features is surveyed using a Trimble GPS Pathfinder system. Because GPS accuracy ranged from 1 to 4 meters, field notes and photos are used to ensure correct relative location of each tree was correct. The location of trees selected for sampling relative to landslide features are shown in Figure 4. One of the sampled trees growing next to a shallow landslide on the landslide toe is shown in Figure 5.

This study utilizes cross dating techniques and growth disturbance analysis methods described in Keck et al. (2014). Three growth disturbances are quantitatively defined by analyzing the ring series of each tree using a double moving window (Figure 6). The three growth disturbances are: release, suppression and eccentric growth (Figure 7). A release growth disturbance can result from the mortality of adjacent trees which

expose a tree to more sunlight, water and nutrients. A suppression growth disturbance may occur if the roots of a tree are sheared or pulled by a tension crack or if the trunk of a tree is buried by debris. Eccentric growth forms in response to tilt. If a tree suddenly tilts, it will try to return to an upright position by growing reaction wood on one side of the tree and suppressed growth on the other. In cross-section, the growth of the tree becomes eccentric rather than symmetric.

Landslide activity is inferred from an event-response index commonly applied in dendrogeomorphic studies of landslides (Shroder, 1978; Lopez et al., 2012; Silhan, 2016) Trees sampled in Keck et al. (2014) were primarily sub-tropical broadleaf trees growing in the Snow Mountain Range of Taiwan. In this study, all trees are temperate conifers growing in the Olympic Mountains. Because tree species, stand conditions and climate are widely different between the Taiwan and the Olympic mountains, the thresholds used to detect a growth disturbance are adjusted to ensure that only landslide triggered growth disturbances are detected by the analysis technique. To adjust the threshold, growth disturbance analysis is conducted on both the landslide sample group and the control group. The thresholds are fine tuned so that trees growing on an unquestionably active landslide feature exhibit a growth disturbance without causing the control group trees to exhibit a growth disturbance.

Years of disturbance in the reference trees that cannot be removed by adjusting the threshold are interpreted as wind disturbance. Years of wind disturbance in the control group are used to help interpret if a growth disturbance in a landslide group tree was wind caused or caused by landslide movement. If a growth disturbance occurred during years of wind disturbance and if that tree is not adjacent to a clearly active landslide feature, the growth disturbance of the landslide tree are assumed to be due to wind and not used to infer landslide activity.

The thresholds used to define a growth disturbance in this study are as follows: A confidence level of 99.75% is used in a paired t-test to determine if changes in average eccentricity are significant; significant suppression and release events need to occur in two of the four radius cores and; the average growth change and year to year growth change must meet the following thresholds:

1. Four year average growth change of at least 50%

$$\left|\frac{M_1 - M_2}{M_1}\right| \times 100\% > 50\% \qquad \text{E.1}$$

2. Year to year change of at least 25%

$$\left|\frac{W_1 - W_2}{W_1}\right| \times 100\% > 25\% \qquad \text{E.2}$$

Where M_1 and M_2 are the average ring width of the two four-year windows and W_1 and W_2 are the width of the two rings being compared for each year in the ring series (Figure 6). An event response index of 20 percent is used to determine years of landslide activity. This value is high relative to other studies (Shroder, 1978; Lopez, 2012; Silhan, 2016); however, trees in this study are selectively sampled based on location of the trees on active features of the landslide to help ensure that movement of the landslide disturbs as many sampled trees as possible. By using this sampling technique and a high event response index, it is assumed that landslide-caused events rather than wind caused events are more likely to be detected.

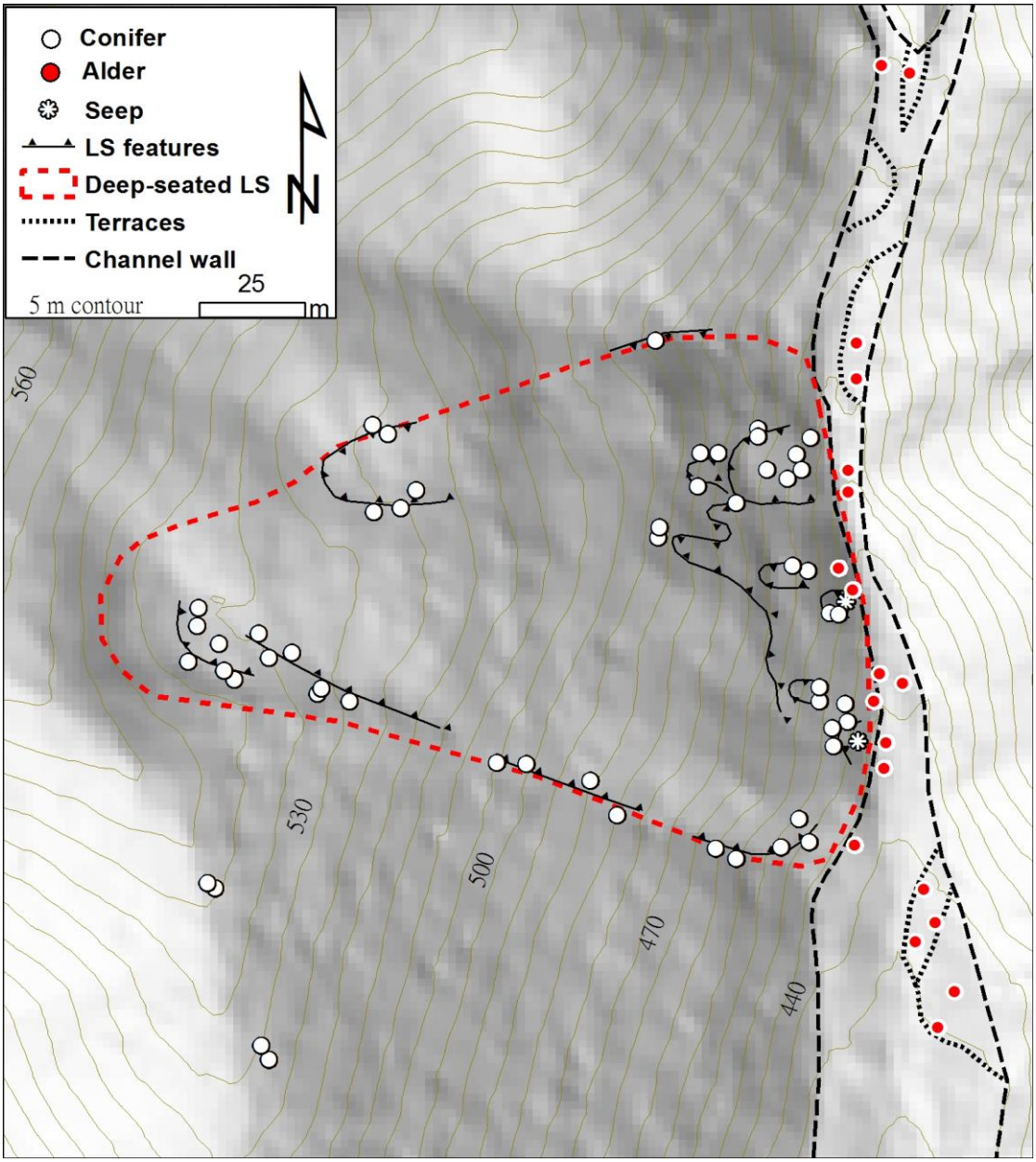

Figure 4. Location of trees relative to landslide and channel features that were used to date landslide and debris flow events. Four trees on ridge are reference trees.

Figure 5. A conifer growing next to a shallow landslide on the toe of the deep-seated landslide.

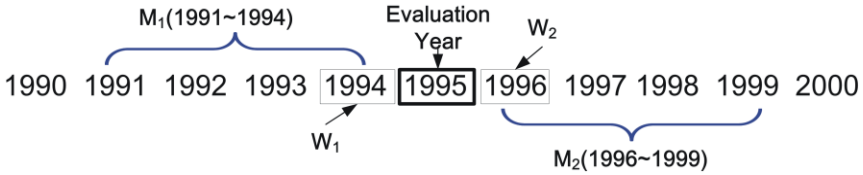

Figure 6. Double moving window technique applied in Keck et al. (2014) and this study.

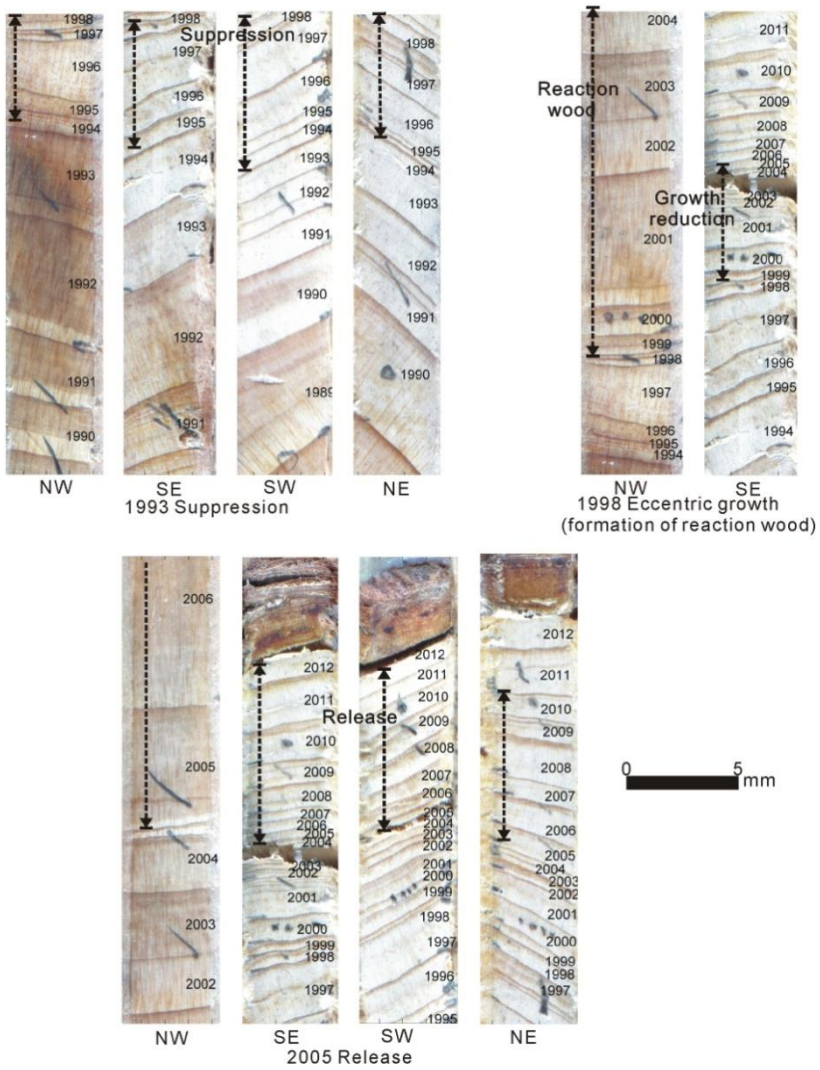

Figure 7. Example of suppression, release and reaction wood formation events in cores extracted from a tree in Keck et al. (2014).

3.3 Harvest and debris flow records

The year and extent of tree harvests and debris flows are determined from orthorectified air photos. Channel scour visible in the air photos is interpretated as evidence of debris flow if the scour initiates at a landslide scar. Debris flows that pass the toe of the landslide are noted. The areal extent of each debris flow is mapped from the air photos. Air photos are from the WA Department of Natural Resources air photo collection and include years 1950, 1960, 1967, 1969, 1971, 1975, 1977, 1979, 1980, 1981, 1985, 1988, 1990, 1992, 1994, 1997, 2003, 2005, 2006, 2009, 2011, 2013 and 2015.

The air photo record does not include every year. In particular, there is a 5 year gap between the 1997 and 2003 photos. Also, the air photos were often recorded in the summer or early fall, before the rainy season. Therefore, the year a debris flow is first

observed in the air photo is not necessarily the year the debris flow occurred.
To help improve the accuracy of airphoto determined years of debris flow activity, the age of the oldest red alders (*alnus rubra*) growing on the debris flow terraces and scoured channel walls next to the landslide toe are used. Alder age is determined from the number of annual rings observable in a core or cross-section extracted from the base of the tree, near the ground surface. Locations of sampled alders relative to debris flow features in the channel are shown in Figure 4. Figure 8 shows how cross-sections were removed from two of the largest alders growing on a debris flow terrace located 30 meters downstream of the right edge of the landslide

Figure 8. Cross-sections are removed from the base of the largest alders growing on a terrace deposit. The annual rings of the alder were examined to determine the tree age and infer the year the terrace formed.

3.4 Water input (rain plus snowmelt) model

3.4.1 Precipitation and temperature forcing data

Precipitation and temperature observations used to compute water input and are extrapolated from the Western Region Climate Center Clearwater Observation Station (WRCC, 2016) to the basin. The WRCC Clearwater precipitation and temperature observations span 1948 to 2016. Daily accumulated precipitation at the basin is computed by multiplying the Clearwater Observation Station daily value by a monthly

precipitation ratio as described in Raleigh and Lundquist (2012). A monthly precipitation ratio is determined for each month by dividing the mean monthly accumulated precipitation at a point near the center of the basin by the mean monthly accumulated precipitation at the Clearwater Observation Station. Mean monthly accumulated precipitation at the two points are derived from 800 meter resolution PRISM 30 year averages of monthly accumulated precipitation (PRISM, 2016). An example of how the precipitation ratio was determined for the month of December is shown in Figure 9.

Daily maximum and minimum temperatures at the basin are estimated by adding the difference between mean monthly temperatures at the basin and the Clearwater River station to the daily temperature recorded at the Clearwater River station. Mean monthly temperature at the two points are determined from 800 meter resolution PRISM 30 year averages of monthly maximum and minimum temperature.

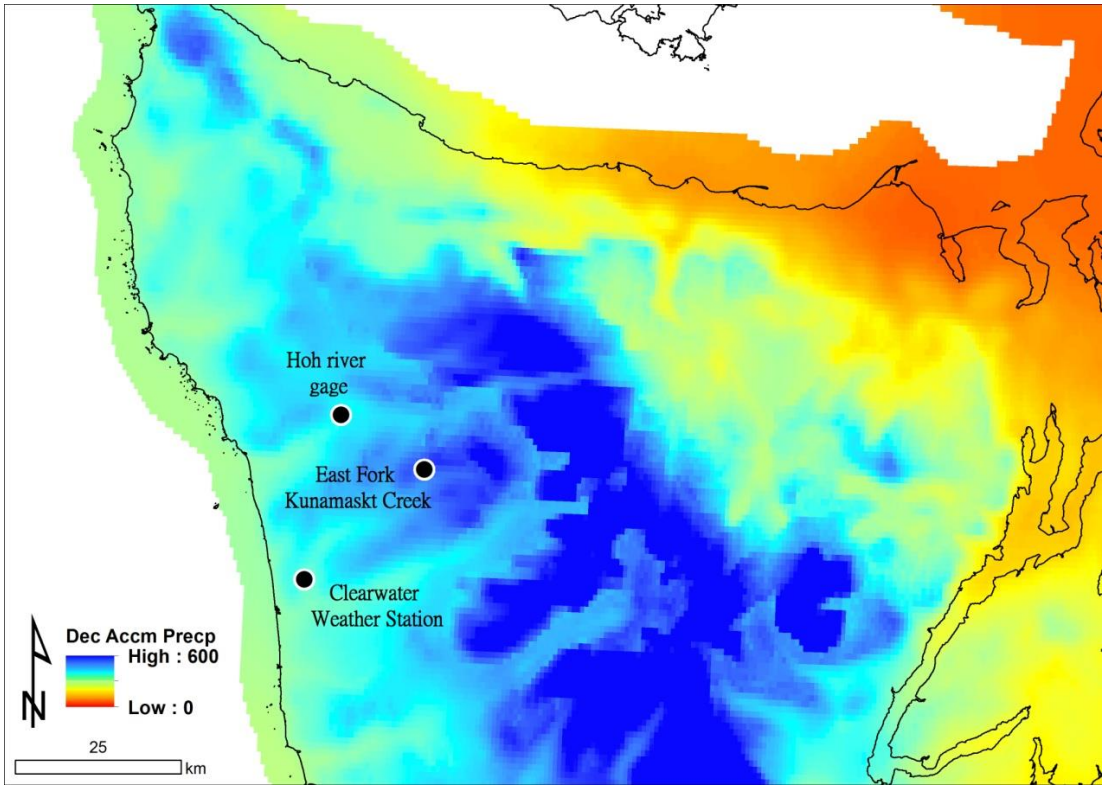

Figure 9. PRISM Mean accumulated precipitation for the month of December and location of the study basin and the Clearwater station gage. Monthly normals for precipitation and temperature were used to extrapolate observations at the Clearwater observation station to East Fork Kunamaskt Creek

3.4.2 Calibrating the snow and ablation model Snow17 to obtain water input

Water input (rain plus snowmelt) is computed from the snow accumulation and

ablation model Snow17. Snow17 is constructed based on a conceptual model of the physical processes that control how rain and snow, vegetation and temperature interact (Anderson, 1976). The output of Snow17 is a daily time series of precipitation.

The National Oceanic and Atmospheric Administration (NOAA) provides guidelines for selecting initial Snow17 model parameters in the National Weather System River Forecast System (NWSRFS, 2016). The NWSRFS guidelines are based on the vegetation and terrain conditions of the basin; however, actual values for each basin are to be determined through model calibration to observations of snow water equivalent (SWE) (NWSRFS, 2016). Because there is no SWE record for the study basin, a range of possible model parameters suitable for the basin is created from the parameters used to calibrate SNOW17 to eleven different SNOTEL stations (NRCS, 2016) located within one degree latitude and five hundred meters of the mean elevation of the study basin (Table 1, Figure 10).

Snow17 was not specifically designed to predict how land use changes affect snow accumulation and melt (Anderson, 2006). The method used in this study for determining vegetation affects on water output and SWE are as follows:

For each station, SNOW17 is calibrated using seven water years of SWE data. In total, there are eleven parameters in Snow17 that can be used to calibrate modeled SWE to observed SWE. Seven of the eleven parameters are assigned a constant value specific to Western Washington based on suggested values (NWRFS, 2016). The other four parameters, which are typically used for calibration (NWRFS, 2016), are calibrated using a “brute force” method: over 700 different combinations of parameter sets are tested; the parameter set that yields the highest Nash-Sutcliffe (NS) value is selected. From the range of parameter values calibrated to the eleven SNOTEL sites, a set of parameter values for forested and cleared conditions is created using NWRFS manual guidelines. Snow17 parameter values for fully harvested and fully forested conditions are listed in Table 2. A description of each parameter is listed in Table 3.

Table 1 Eleven SNOTEL sites used to develop Snow17 parameter values for basin

Station name	Description of vegetation	Lat.	Long.	El. [m]	Annual precip [mm]	Mean temp [C]	Max temp [C]	Min temp [C]
Marten Ridge	100% coniferous tree farm harvested around 1995	48.7667	-121.7000	1072.9	3263.3	6.5	10.3	2.8
ElbowLake	100% coniferous tree farm harvested ~30-50 years ago	48.6833	-121.9167	926.6	3453.7	7.6	12.2	2.9
Alpine meadows	85% coniferous forest, 15%	47.7833	-121.7000	1066.8	4026.6	5.8	9.6	1.9

	meadow does not appear to have ever been harvested							
Buckinghorse	75% coniferous forest, thin rocky soils, just below treeline on ridge, never harvested	47.7167	-123.4500	1484.4	2303.2	6.0	10.0	1.9
Skookum Creek	100% coniferous tree farm harvested around 1995	47.6833	-121.6167	1008.9	3556.8	6.9	10.7	3.1
Mt Gardner	Near boundary of 100% coniferous tree farm harvested around 1995	47.3500	-121.5667	1070.0	2512.1	7.7	13.0	2.5
Tinkham Creek	100% coniferous tree farm > 40 year old plantation	47.3333	-121.4667	911.4	2713.2	6.0	10.4	1.6
Meadows Pass	100% coniferous tree farm harvested ~20-40 years ago	47.2833	-121.4667	984.5	2470.9	5.9	10.2	1.7
Cougar Mountain	100% coniferous forest, possibly never harvested	47.2833	-121.6667	975.4	2563.5	6.8	11.1	2.5
Hucleberry creek	Christmas tree farm from 2003 to 2014	47.0655	-121.5877	685.8	1095.9	7.0	12.4	1.6
Mowitch	100% coniferous tree farm harvested and planted around 2003	46.9333	-121.9500	963.2	1774.8	6.7	11.1	2.4
East Fork Kunamaskt Ck	100% coniferous tree farm harvested ~20-40 years ago	47.7432	-124.0663	650.0	3600.0	9.5	14.0	5.0

Table 2 Snow17 parameters for fully forested and fully harvested conditions

Cond.	SCF	UADJ	MBASE	MFMAX	MFMIN	TIPM	NMF	PLWHC	PXTEMP1	PXTEMP2	PXTEMP
Forested	1	0.0001	0.06	0.7	0.4	0.15	0.15	0.1	0	3	1.5
Harvested	1.25	0.08	0.06	0.7	0.1	0.15	0.15	0.1	0	3	1.5

Table 3 Description of each Snow17 parameter

Parameter	Description
SCF	Gauge under-catch snow correction factor
UADJ	Average wind function during rain on snow [mm/mb]
MBASE	Base temperature above which melt typically occurs [□]
MFMAX	Maximum melt factor during non-rain periods [mm/□/6 hr]
MFMIN	Minimum melt factor during non-rain periods [mm/□/6 hr]

TIPM	Used to compute temperature in the snow near the surface
NMF	Maximum negative melt factor [mm/□/6 hr]
PLWHC	Percent liquid water holding capacity of the snow pack
PXTEMP1	Lower Limit Temperature dividing transition from snow, [□]
PXTEMP2	Upper Limit Temperature dividing rain from transition, [□]
PXTEMP	Temperature dividing rain from snow, [□]

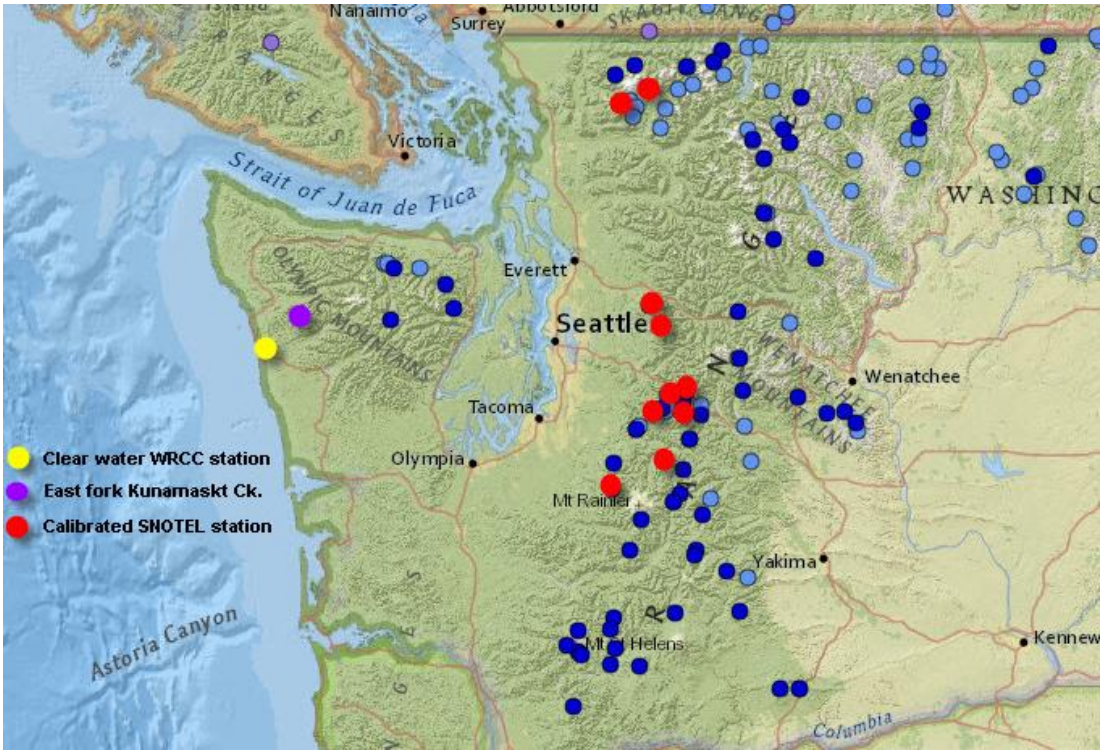

Figure 10 Map of SNOTEL stations used to determine parameter values for forested and non-forested sites. Map modified from NRCS (2016). Blue dots are other SNOTEL stations not used in this study

3.5 Modeling stream response to harvest

Runoff from the basin outlet is modeled using the lumped hydrologic model BGM (Bucket Grassland Model, Istanbullouglu et al, 2012). Predicting flow with BGM involves three components: (1) developing three years of daily flow observations at the outlet of the basin over the observation period (2013 to 2016); (2) Calibrating the lumped hydrologic model to fully forested conditions using temperature and water input as forcing variables; (3) Re-running the calibrated model using a set of model parameters representative of fully harvested condition.

3.5.1 Flow observations

A continuous record of flow observations is developed from rating curves fit to sixteen discharge and stage measurements and a continuous record of stream stage collected at the basin outlet (Figure 1) between October, 2013 and July, 2016. The deep-seated landslide is located 1,700 meters upstream of the outlet. Because the hydrograph of steep, bedrock watersheds like the study basin are generally dominated by rapid-subsurface runoff (Harr, 1977), it is assumed that changes in flood frequencies predicted at the basin outlet also occur throughout the watershed and at the base of the landslide.

During the three year observation period, aggradation occurred locally at the gage and caused the geometry of the channel to change. Because a single rating curve is only applicable to a single channel geometry, a series of rating curves was required to accurately convert the gage record to a discharge record. Each rating curve is constructed using methods described in Rantz et al. (1982).

The series of rating curves are developed based on the assumption that the ratio of cumulative run-off from the basin outlet to cumulative precipitation into the basin (R/P) is constant over time. A R/P value of 0.76 is used which corresponds to a evapotranspiration to precipitation ratio (ET/P) of 0.24. This ET/P value is based on observations on Vancouver island (Jassal, 2009) and is consistent with evapotranspiration rates computed using the ASCE method for calculating radiation and Priestly Taylor method for potential ET adjusted to actual evapotranspiration rates determined in Shinker and Bartlein, (2010). Implicit in this assumed R/P value is that the only loss of water from the basin is via evapotranspiration and runoff out the basin outlet. Also, this R/P value is based on the assumption that the only source of water into the basin is water input from precipitation falling into the basin.

Developing the rating curves in this way results in five rating curves that show a trend of localized aggradation equivalent to several centimeters per year over the three-year observation period (Figure 11) A plot of accumulated precipitation and runoff determined from the five rating curves (each rating curve applies to a different period of time) is shown in Figure 12.

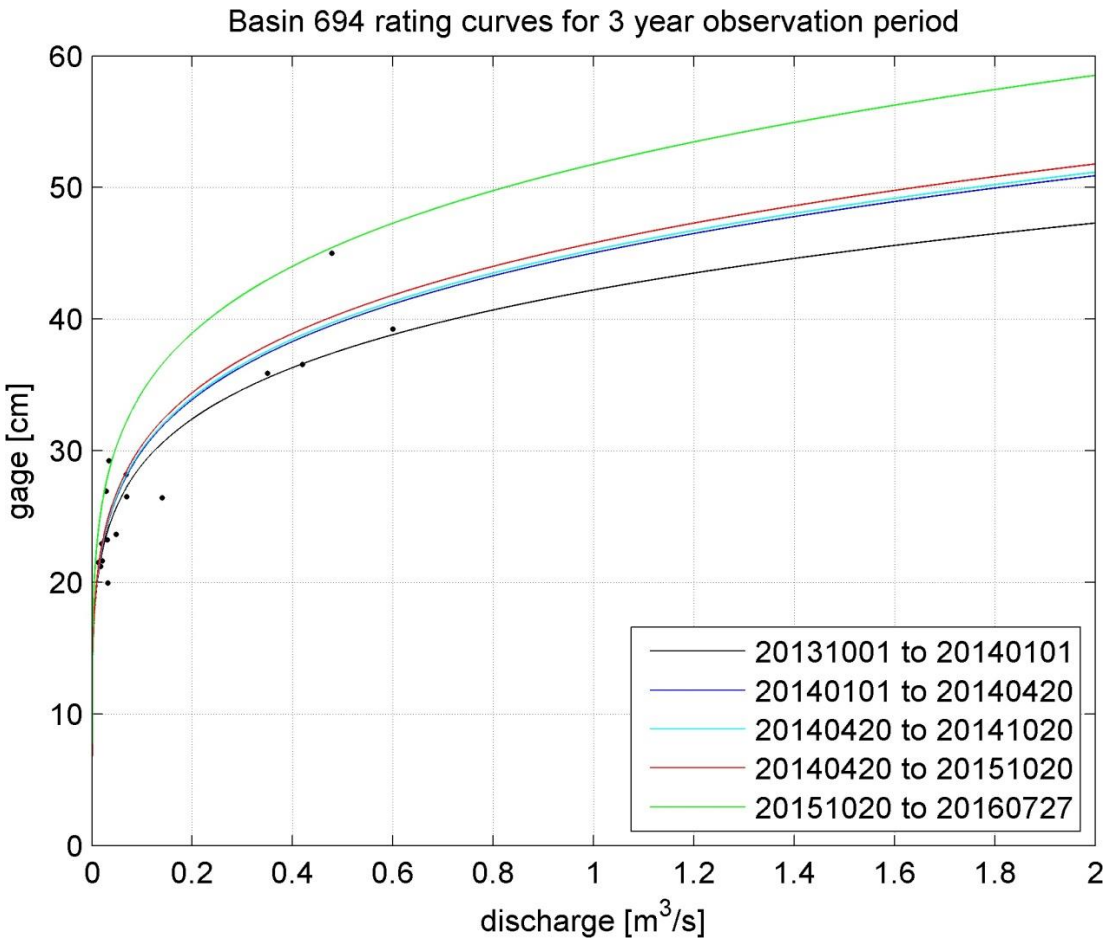

Figure 11 Rating curves that result from trying to maintain a constant ratio of accumulated precipitation vs accumulated runoff.

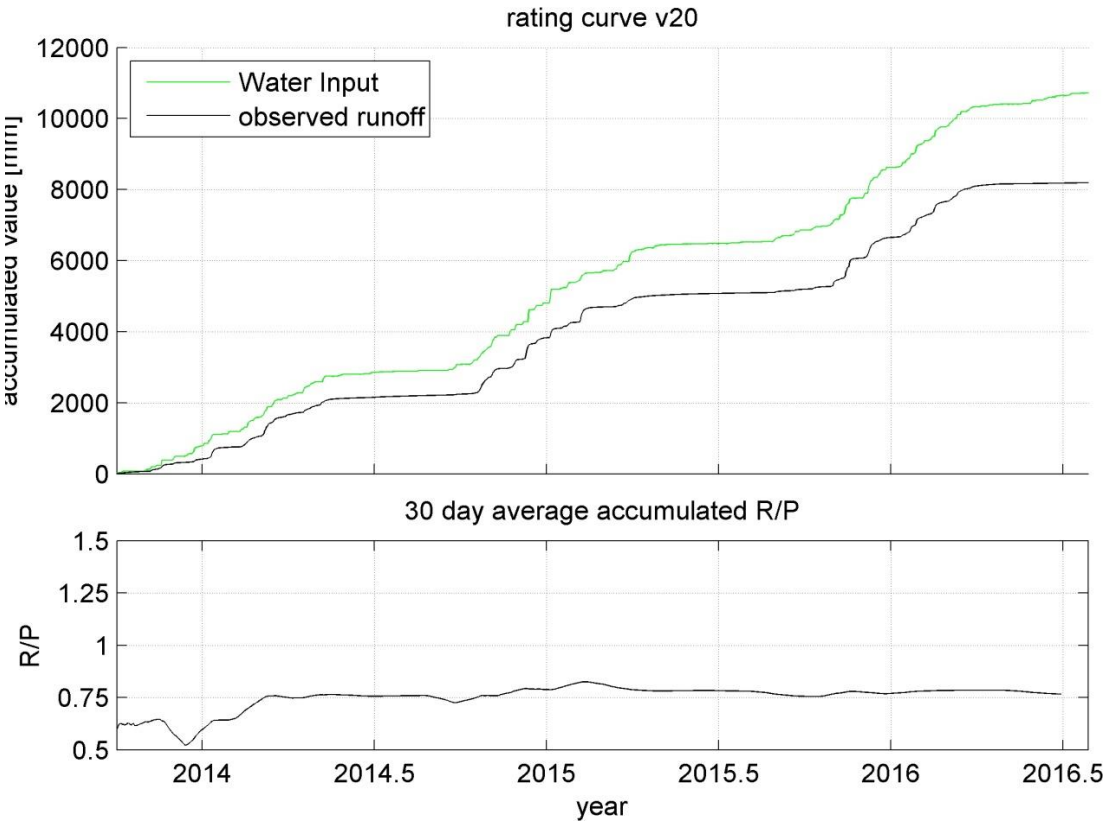

Figure 12 Top: Accumulated precipitation and observed runoff. Bottom: Plot of the ratio of accumulated runoff versus accumulated precipitation (R/P).

3.5.2 Calibrating the basin-scale hydrologic model BGM

BGM consists of a bucket-hydrology modeling component and a vegetation dynamics modeling component. The vegetation dynamics component produces a time series of leaf area index (LAI) that is input into the bucket hydrology modeling component. In this study, the vegetation dynamics component is turned off and instead a time series of constant LAI values is used. For fully forested conditions, an LAI value of 5 (Jassal et al., 2009) is used to represent a full canopy of mature coniferous trees. For fully harvested conditions, an LAI value of 0.1 is used to represent sparse grass and shrubs.

The bucket-hydrology modeling component includes processes for canopy interception, evapotranspiration, infiltration, surface runoff, subsurface flow and bedrock flow. Specifics on how each process is modeled is detailed in Istanbullouglu et al. (2012). A summary of the modeling methodology is included below.

The amount of water reaching the soil surface is controlled by precipitation rates, canopy interception and snow pack dynamics. Canopy interception is determined as the minimum of an assumed interception depth multiplied by the vegetation cover fraction or the precipitation rate multiplied by the cover fraction. Once precipitation exceeds the interception rate, through-fall occurs at a rate equal to the precipitation

rate. The time required for the precipitation rate to exceed the interception rate reduces the overall length of the precipitation event reaching the ground surface.

Conservation of water in the root zone is controlled by a balance between infiltration, saturation excess runoff, evapotraspiration and drainage to bedrock. The amount of water that can be stored in the root zone is larger for thicker and more porous soils.

Infiltration rate is the minimum value of the precipitation rate and potential infiltration rate. Potential infiltration rate is controlled by soil moisture and permeability. Once the soil column is saturated, the infiltration rate is controlled by the drainage rate to bedrock. The drainage rate is computed using the saturated hydraulic conductivity of the soil. For unsaturated conditions, the Campbell Soil Moisture Retention Model is used to determine the drainage rate. The lower boundary of the root zone is assumed to be described by a unity hydraulic gradient.

Actual evapotranspiration is computed using a soil moisture limitation method; a coefficient between 1 and 0 is multiplied by the potential evapotranspiration rate. Potential evapotranspiration is determined using the ASCE method for calculating radiation and Priestly Taylor method for potential ET. The coefficient is determined as defined in Liao et al., 2001.

In BGM, there are a total of twelve parameters. Of those twelve, five parameters are selected based on published values and maximum values that are suitable for fully forested conditions. The additional seven parameters are adjusted to calibrate the model to the flow observations at the basin outlet: CIC, Fveg, Zr, bshape, Tsub, Tbase and Fg. Each of the twelve parameter is described in Table 5.

The seven calibration parameters are calibrated using a “brute force” method. BGM is run for over 10,000 different combinations of the parameter values and a NS value and Root-Mean-Square (RMS) error for each combination is computed. From the results, the combination of parameter values that results in a high NS value and low RMS error value is selected. As an additional check that the modeled hydrograph adequately predicts the observed hydrograph, the baseflow component of observed flow and modeled flow are estimated using a recursive filter (Nathan and McMahon, 1990) and compared to ensure consistency. Parameter values that optimized model performance are listed in Table 4.

Through this process, the model is calibrated. Baseflow residence time is 220 days and sub-surface residence time is 1.7 days. Model performance over the observation period is illustrated in Figure 13 and detailed in Table 5. The base flow index of the modeled hydrograph and the base flow index of the observed hydrograph are comparable at 0.108 vs 0.112.

Table 4. BGM Parameter values that result in highest NS and lowest RMS values

Soil type	CIC	Fbare	Fveg	Zr	bshape	Tsub	Tbase	Ini-store	Inistore-ground	Fg	LAI-max
1	1.6	0.3	2	0.65	0.00000001	1.7	220	3	20	0.11	5

Table 5 Description of each BGM parameter

Parameter	Description
Soil type	Soil type 1: high hydraulic conductivity, low field capacity
CIC	Controls the amount of precipitation that is lost to interception and evaporation
Fbare	Affects the ratio of water that is lost to evaporation from the soil surface
Fveg	Affects the amount of water that is lost to transpiration
Zr	Regolith depth
bshape	Affects how much water is transported as surface runoff
Tsub	Residence time of the subsurface flow
Tbase	Residence time of base flow
Inistore	Initial storage in subsurface flow
Inistoreground	Initial storage in base flow
Fg	Ratio of infiltration that reaches the bedrock
LAImax	affects the amount of water that is lost to transpiration

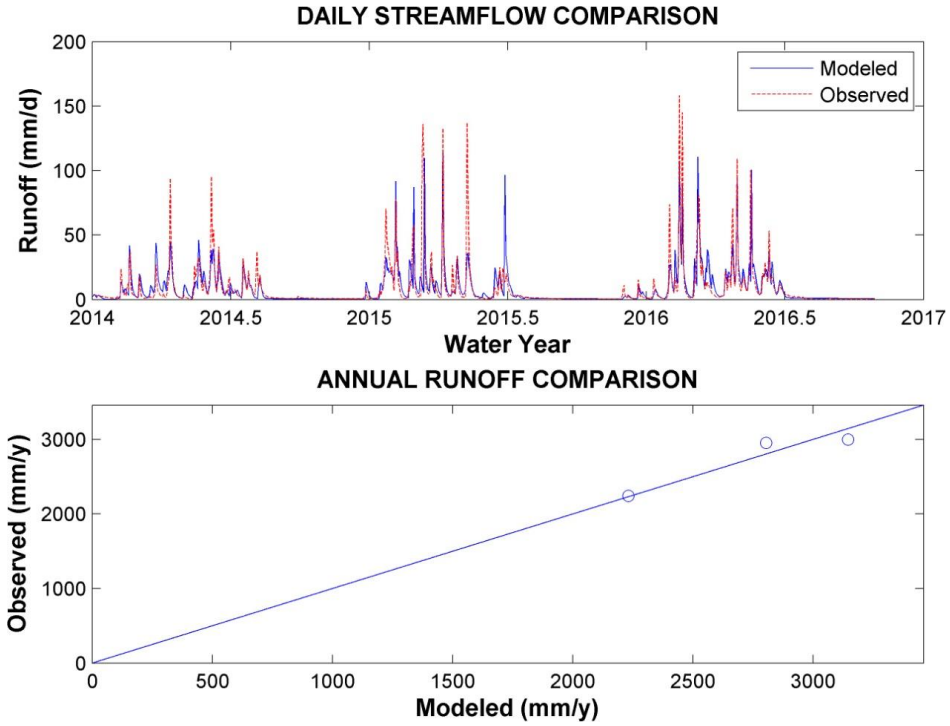

Figure 13 Model performance over three year calibration period

Table 6 BGM model performance over three year calibration period

Daily Nash Sutcliffe value	0.57
Weekly Nash Sutcliffe value	0.79
Monthly Nash sutcliffe value	0.88
Difference in accumulated flow [mm]	-4.56
Drainage ratio	0.70
Interception ratio	0.07
Evapotranspiration ratio	0.23
Runoff ratio – observed	0.76
Runoff ratio – modeled	0.76
Surface runoff ratio	0.07
Subsurface ratio	0.84
Ground water ratio	0.09

3.5.3 Modeling flow from fully forested and fully harvested conditions

Four parameters are used to adjust the model from fully forested to fully harvested conditions: CIC, Fbare, Fveg and LAImax. Each parameter is described in Table 5. Parameter values are selected based on published values and maximum values that are suitable for fully harvested conditions. The value of each BGM parameter used to represent forested and harvested conditions are listed in Table 7.

Table 7 BGM parameter values for fully forested and fully harvested conditions

Condition	CIC	Fbare	Fveg	Zr	bshape	Tsub	Tbase	Inistore	Inistoreground	Fg	LAImax
Fully forested	1.6	0.3	2	0.65	0.00000001	1.7	220	3	20	0.11	5
Fully Harvested	0.05	0.8	1	0.65	0.00000001	1.7	220	3	20	0.11	0.1

3.6 Determining harvest effect on water input and peak flows

Once calibrated, Snow17 and BGM are used to model daily water input and flow at the basin using the 69-year long record (1948 to 2016) of daily precipitation and temperature extrapolated from the WRCC Clearwater station to the basin. This is done for both fully forested and fully harvested conditions. From the time series of daily water input and flow, a 69-year long annual maximum series (AMS) of water input and flow are created. Harvest effects are then quantified by comparing the magnitude of specific return period events. Return period is determined by ordering the AMS from largest to smallest and then computing the reciprocal of the probability of exceedance. Probability of exceedance is computed using a Weibull plotting position. Because several studies have suggested that deep seated landslides may be triggered

by long periods of large antecedent moisture (Iverson and Major 1987, Iverson, 2000, GEER, 2014), an AMS of one-day and thirty-day accumulated events are created for water input and flow for both vegetation conditions.

To determine if peak flows or water input significantly change after harvest in 1990, the 1948 to 1990 AMS for fully forested conditions is compared to the 1991 to 2016 AMS for fully harvested conditions using a rank-sum test and two-pair t-test at a 95% confidence level. A significant change in water input or flow is interpretated to be caused by the harvest so long as precipitation does not also significantly change around the time of the harvest. If precipitation also changes around the time of harvest, then changes in water input are not interpretated as being caused by the tree harvest.

Finally, to determine if water input and flow from fully forested conditions is different from water input and flow from fully harvested conditions over the 69-year long modeling period, the entire AMS of each vegetation condition are compared using a sign rank test and paired t-test and a 95% confidence level.

3.7 Landslide sensitivity to scour and pore-water pressure

Sensitivity to scour and pore water pressure is examined using a two-dimensional slope stability model of the landslide in Slope/W. Slope/W is a slope stability modeling component of the software package Geostudio that is licensed for engineering consulting use (Geostudio, 2016). In Chung et al. (2017), Slope/W was used to model landslide sensitivity to precipitation and identify a landslide activity rainfall threshold.

To model the stability of a slope, the user inputs the geometry of the slope, the geometry of the subsurface conditions, strength properties of each geologic unit and soil water conditions. The user must also select a factor of safety (FS) computation method and delineate the entrance and exit extents of the surface of rupture. Strength properties include the internal angle of friction, cohesion and density. Subsurface conditions include the orientation and thickness of each geologic unit, the location of the surface of rupture and the location of the phreatic surface.

In this study, because the landslide is in a remote location accessible only by foot, borehole information that might help interpret the subsurface conditions and the location of the surface of rupture does not exist. Instead, a conceptual model of the subsurface conditions is developed based on field observations of the landslide and on a cross-section of the landslide overlayed with a cross-section of the intact hillslope. The landslide cross-section is measured from the crown to the toe along the center of the landslide. The intact slope cross-section is measured 80 meters downstream of the landslide parallel to the landslide cross-section (Figure 14).

Because the direction of landslide motion is perpendicular to the dip of the bedding,

bedrock orientation does not appear to control landslide motion or geometry. Moreover, bedrock is chaotically fractured and predominately consists of the low-strength, massive beds of siltstone, therefore, landslide motion may not be controlled by any particular set of joints either. Instead, motion may be occurring in the fractured rock much as it would in a sedimentary or granular deposit. The symmetric, rotational appearance of the landslide supports this hypothesis.

Based on these observations, a rotational failure mode that is unaffected by any joint or bedding plane is used for the conceptual model of the landslide. Sensitivity analysis is performed using two versions of this conceptual model. The difference between the models is whether or not the surface of rupture is fixed and the location of the impermeable surface that controls the water table height. Both conceptual models are shown in Figure 15.

In the first model, landslide motion is controlled by a single, fixed surface of rupture that does not change with scour width into the toe. The surface of rupture also serves as the impermeable boundary so that any changes in the water table immediately affect pore water pressures within the landslide. The surface of rupture begins tangent with the head scarp and ends at the right bank of the channel and has a shape that is defined by the least stable geometry. The least stable rupture surface is determined from Slope/W.

In the second conceptual model, landslide motion is controlled by a surface of rupture that migrates into the hillslope as lateral scour into the toe increases. Like the first conceptual model, the surface or rupture begins tangent with the headscarp of the landslide but as scour width into the toe increases, the length of the landslide decreases and the slope of the surface of rupture increases. Also, in conceptual model two, the impermeable surface that is controlling the water table is independent of the surface of rupture and located below it. In other words, the landslide is well drained and does not build up pore water pressures until the water table rises above the surface of rupture. Such a condition might arise if current landslide activity is occurring within the body of a relict, earthquake triggered landslide or within fractured bedrock associated with past activity at the possible fault.

Strength parameters of fractured interbedded sandstone and siltstone (high strength) and fractured siltstone (low strength) measured at a nearby landslide study (Badger, 2007) are used to define the strength of the landslide material (Table 8). The WADOT angle of friction values are typical of weathered soft rock or discontinuities in hard rock which matches field observations but the cohesion values are low and are more typical of clay or soil (Wyllie and Mah, 2005).

The Morgernstern-Price method of slices is used to compute a minimum factor of safety (FS). The Morgernstern-Price method is used because both force and moment

equilibrium are met and because the resulting FS is conservative relative to other methods such as Bishops simplified method of slices that do not consider shear inter-slice forces (Geo-slope, 2016). For each scenario, FS is computed for three phreatic surfaces, six landslide toe configurations and the two WADOT strength parameter sets. Phreatic conditions vary from a water table depth of 0, 10 and 20m above the impermeable surface. These values are within the range of fluctuation observed at the WADOT landslide (Badger, 2007). Toe configurations vary from a lateral scour width of 0 m to a lateral scour width of 25 m into the landslide toe, in 5 m increments. In total, 72 different scenarios are examined. From the resultant plot of FS as a function of lateral scour width and water table depth, landslide sensitivity to scour and pore-water pressures is examined.

Table 8. High and low strength slope stability parameters sets

Condition	Parameter	Value	Source
High strength bedrock Silt-stone and sandstone	Cohesion [kPa]	30	WADOT 2007 XL-2953
	Angle of friction [degrees]	27	
	Unit weight [kN/m3]	22	
Low-strength bedrock – fractured silt-stone	Cohesion [kPa]	20	
	Angle of friction [degrees]	25	
	Unit Weight [kN/m3]	22	

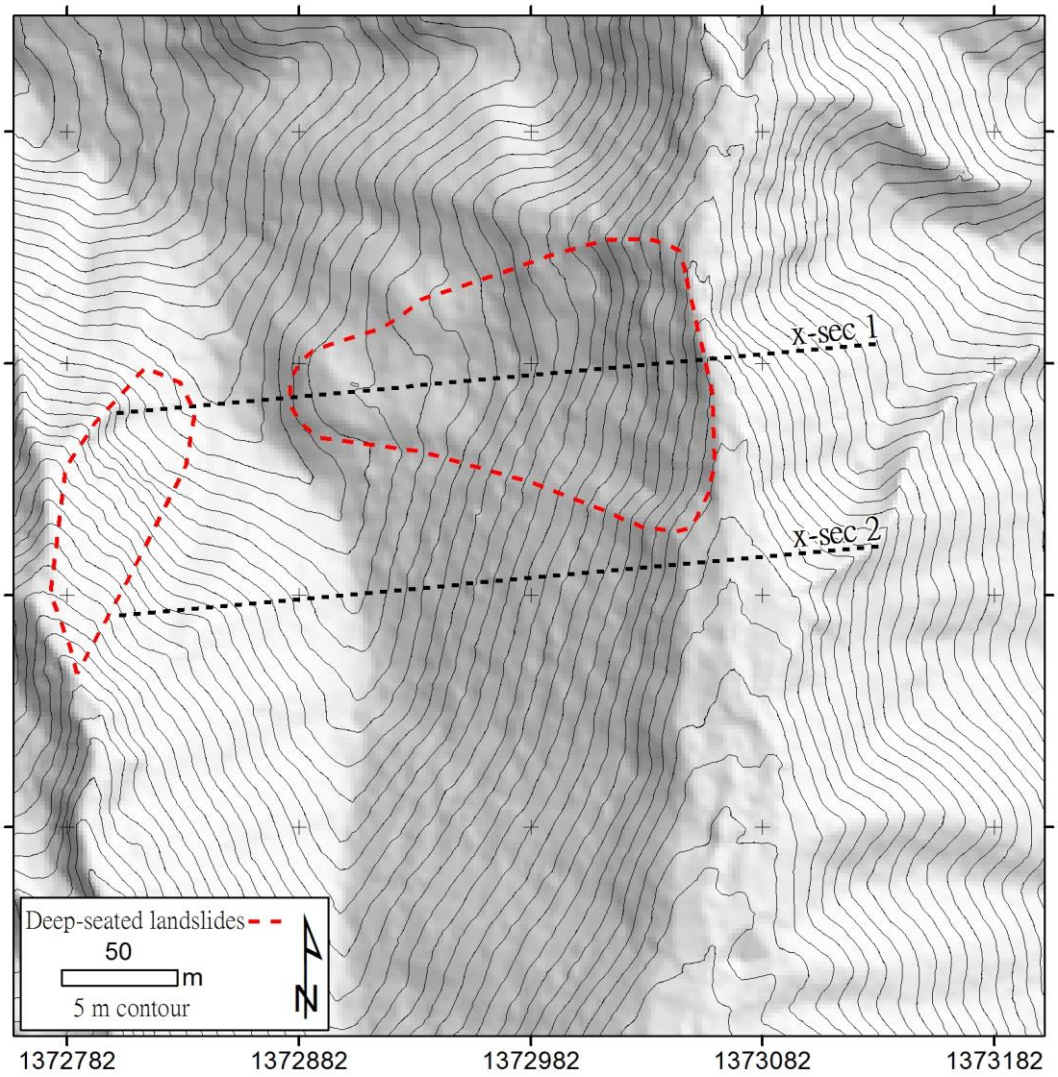

Figure 14 Cross-section locations

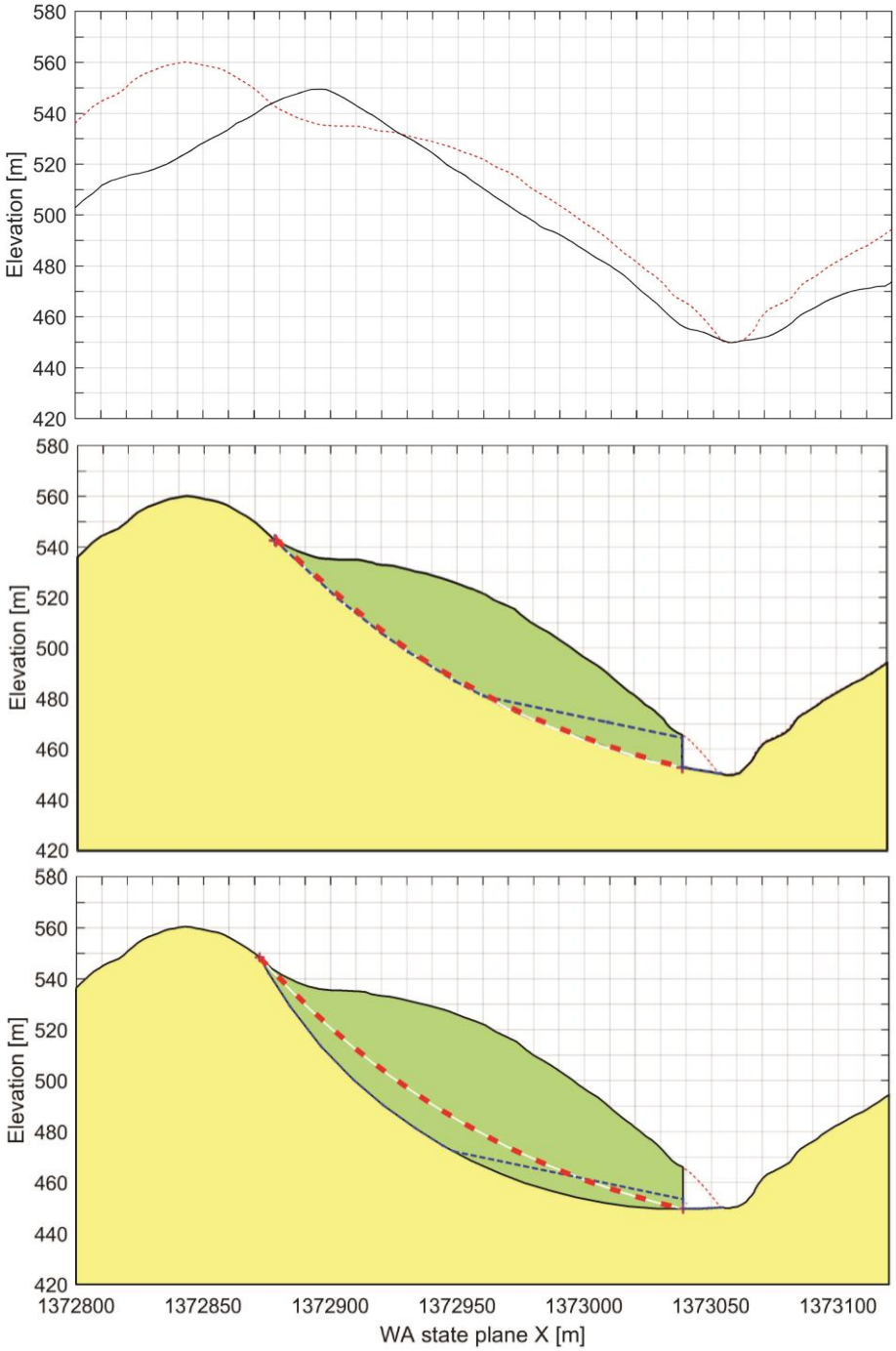

Figure 15 Two conceptual models of the landslide surface of rupture and the location of the impermeable layer controlling the height of the water table. Top - Overlay of cross sections from Figure 14 of landslide and undisturbed slope used to develop conceptual models. Middle – Conceptual Model 1: Water table (dashed blue line) is controlled by impermeable boundary that coincides with surface of rupture (dashed red line) at the base of the landslide, any changes in water table affect stability. Bottom- Conceptual Model 2: water table is controlled by impermeable surface below surface of rupture and changes in water table do not affect landslide stability until water table extends above surface of rupture.

4. Results

4.1 Harvest history

The first harvest and the only road construction in the basin occur in 1967 along a ridge at the northern edge of the watershed. Later, in the 1970's and 1980's, the lower half of the basin was harvested. Trees growing on the landslide and 250 meters upstream of the landslide were harvested in 1981. The head waters of the basin were harvested in 1988 and 1990. To this day, about two thirds of the original forest has never been harvested. Harvest year and location upstream of the deep-seated landslide are shown in Figure 16. Harvest area by year is plotted in Figure 17.

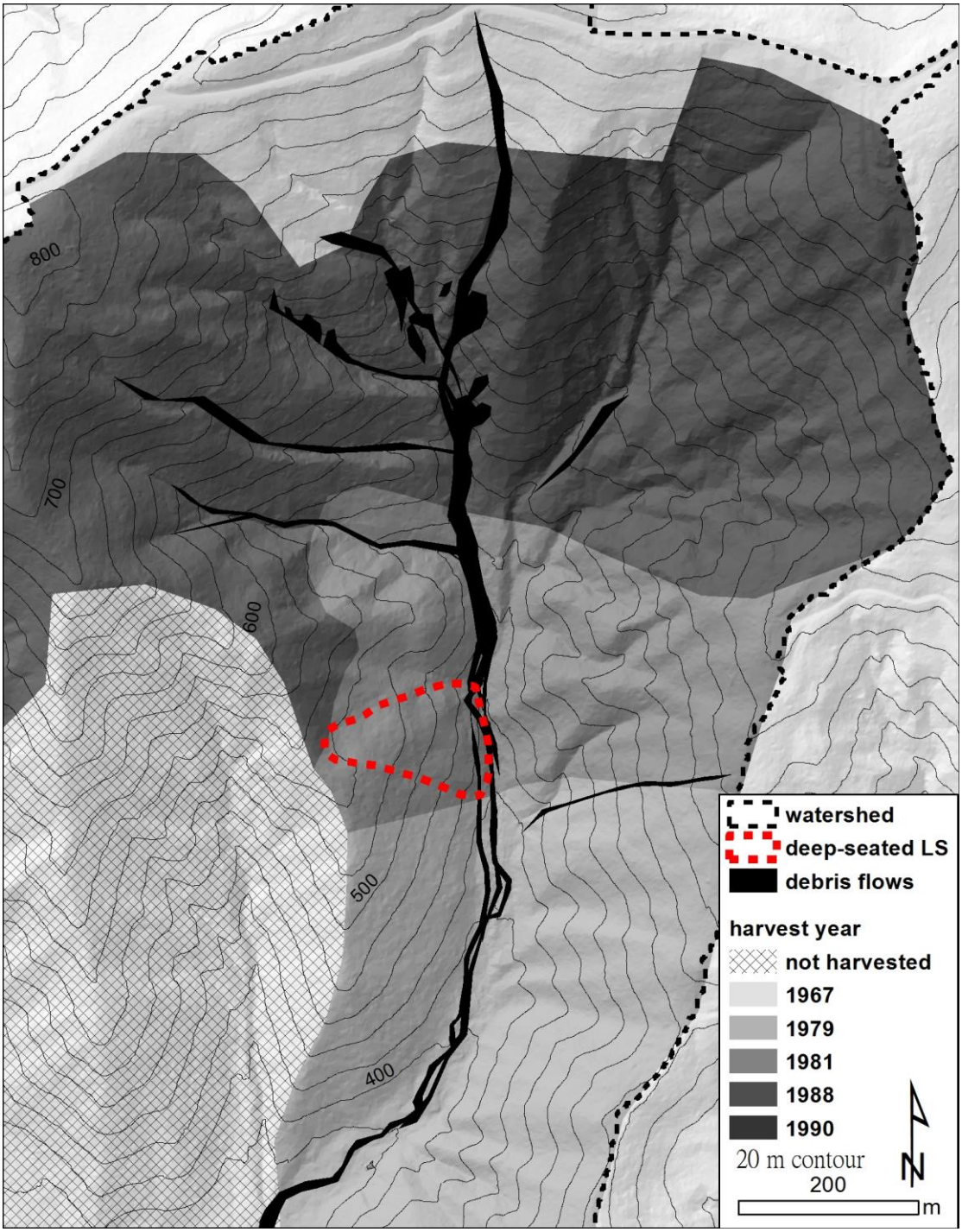

Figure 16 Harvest location and debris flow activity between 1960 and 2015 in channel that flows past deep-seated landslide.

4.2 Debris flow history

Debris flows occur throughout the basin but most are sourced from the headwaters upstream of the deep-seated landslide (Figure 16). In the early 1990's, debris flow frequency and area scoured by debris flows dramatically increases. With the exception

of one debris flow that began as a small landslide in the fillslope of the road constructed along the headwaters of the basin, most debris flows began as small landslides along the channel wall.

Debris flows pass the toe of the deep-seated landslide on or a few years before 1960, 1967, 1992, 2003, 2006 and 2009. Origination years of the alders include 1999, 2000, 2002, 2004, 2007, 2008 and 2009. It is during the 6 year photo gap that the oldest alders originate (Figure 17). The oldest alders were found on one of the higher debris flow terrace deposits and along the upper edge of the channel wall and may have germinated following a debris flow that past the landslide toe around 1998.

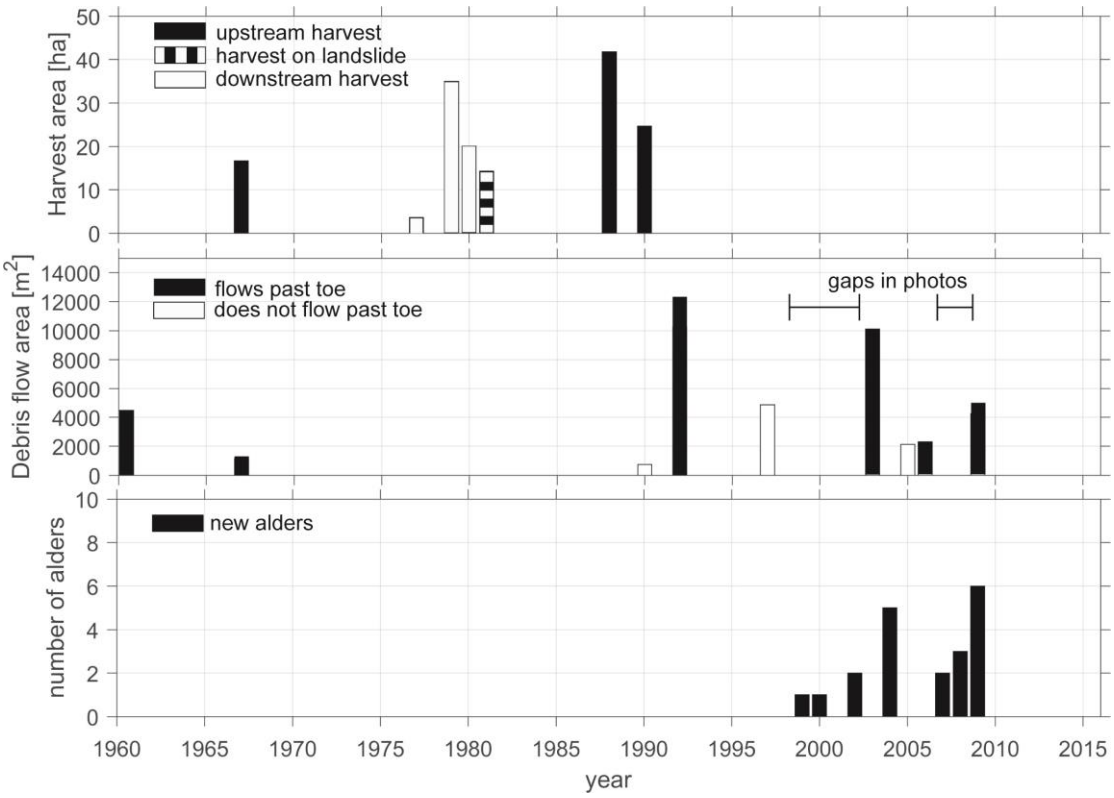

Figure 17 Harvest area, debris flow area and origination year of alders

4.3 Deep seated landslide activity

Over 20% of the landslide sample group exhibits growth disturbance during three periods: 1998 and 1999, 2003 and 2004 and 2009 (Figure 18). In all three instances, the location of the disturbance is along the toe and the right lateral margin of the body and head (Figure 19-21). Growth disturbances also occur along the left edge of the head during the 1998-1999 and 2009 periods of activity. In Figures 19 through 21, growth disturbances are shaded according to growth disturbance type.

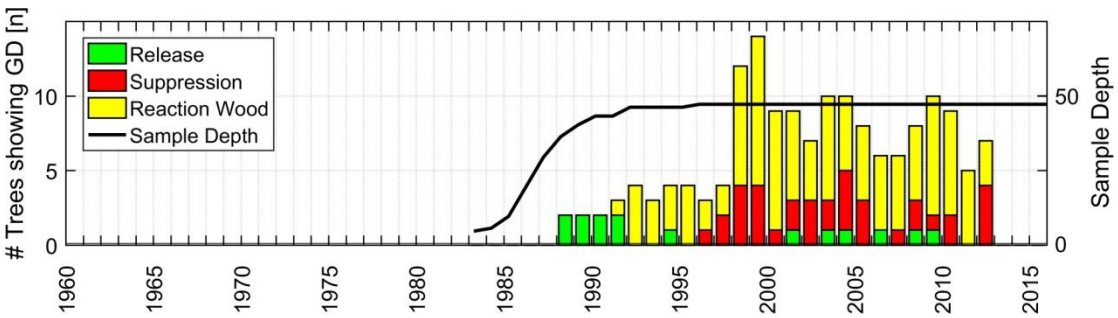

Figure 18 Number of trees showing growth disturbance for each year. Black line is sample depth, scaled to equal an event-response index value of 20%. Years that the number of trees exhibiting a growth disturbance exceeds 20% are interpreted as possible landslide activity years.

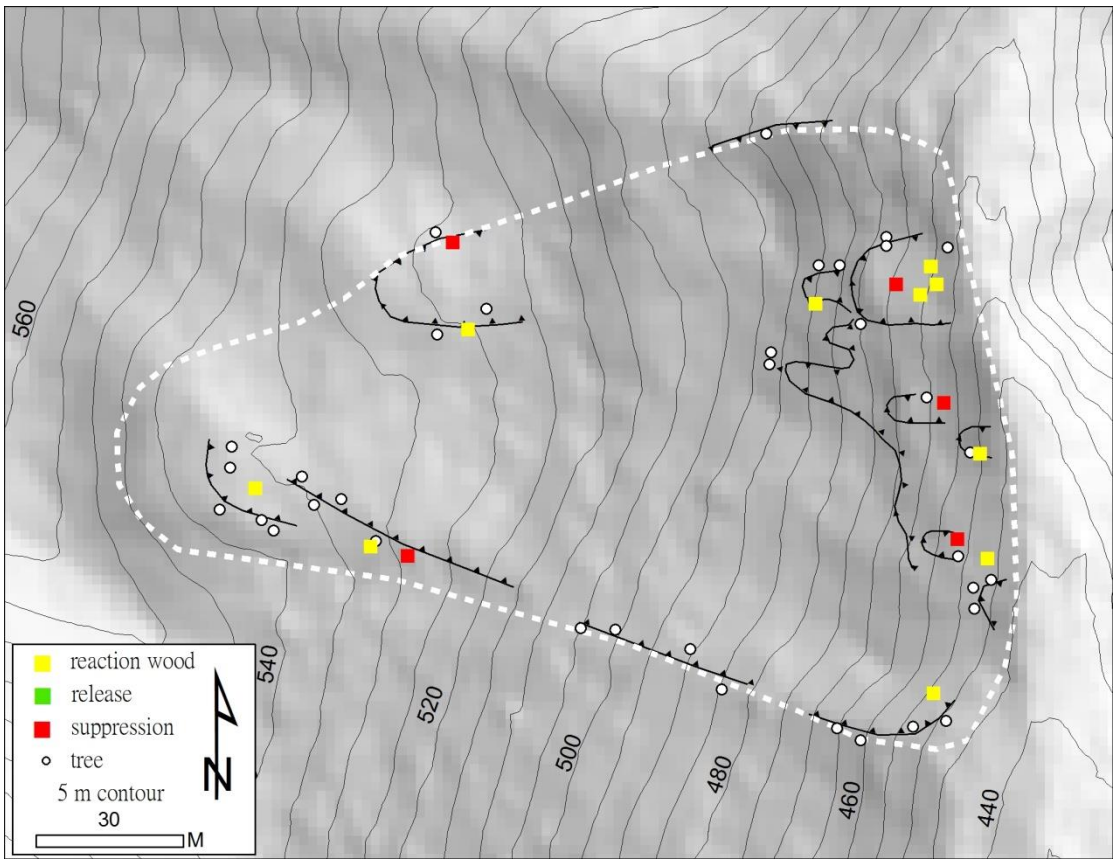

Figure 19 1998 and 1999 growth disturbance location and type

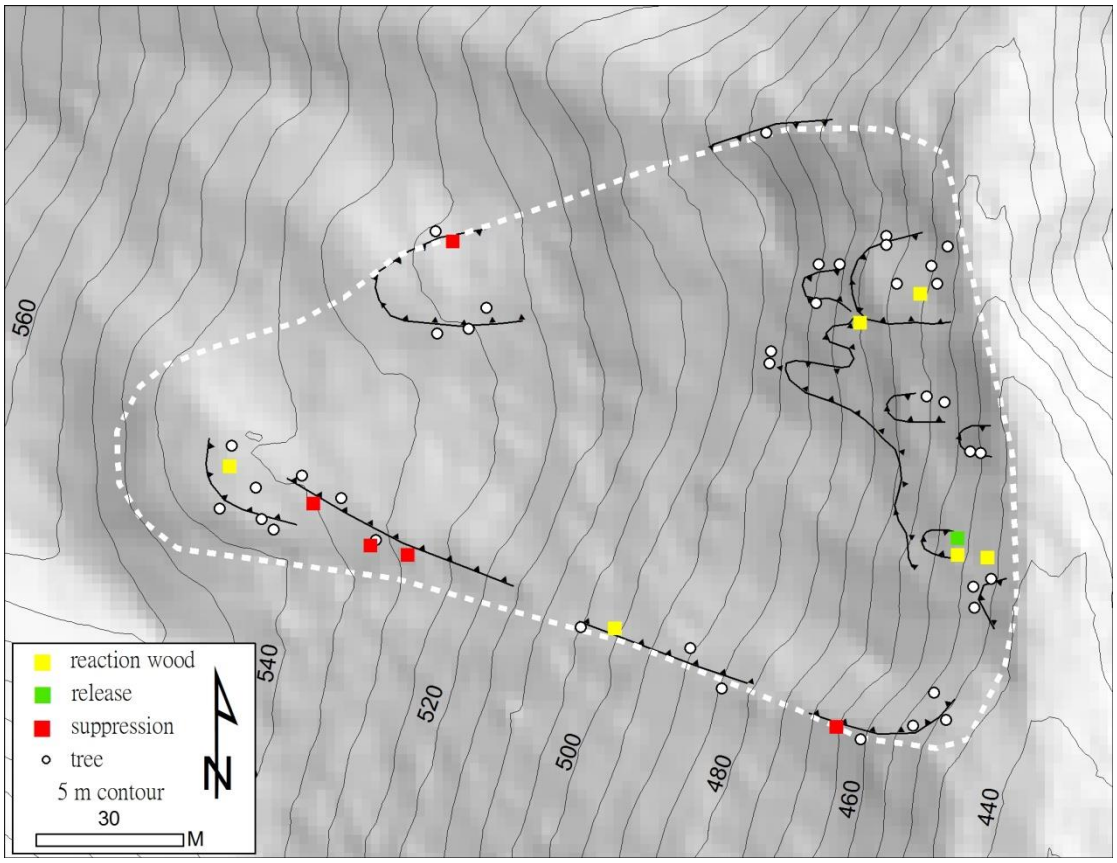

Figure 20 2003 and 2004 growth disturbance location and type

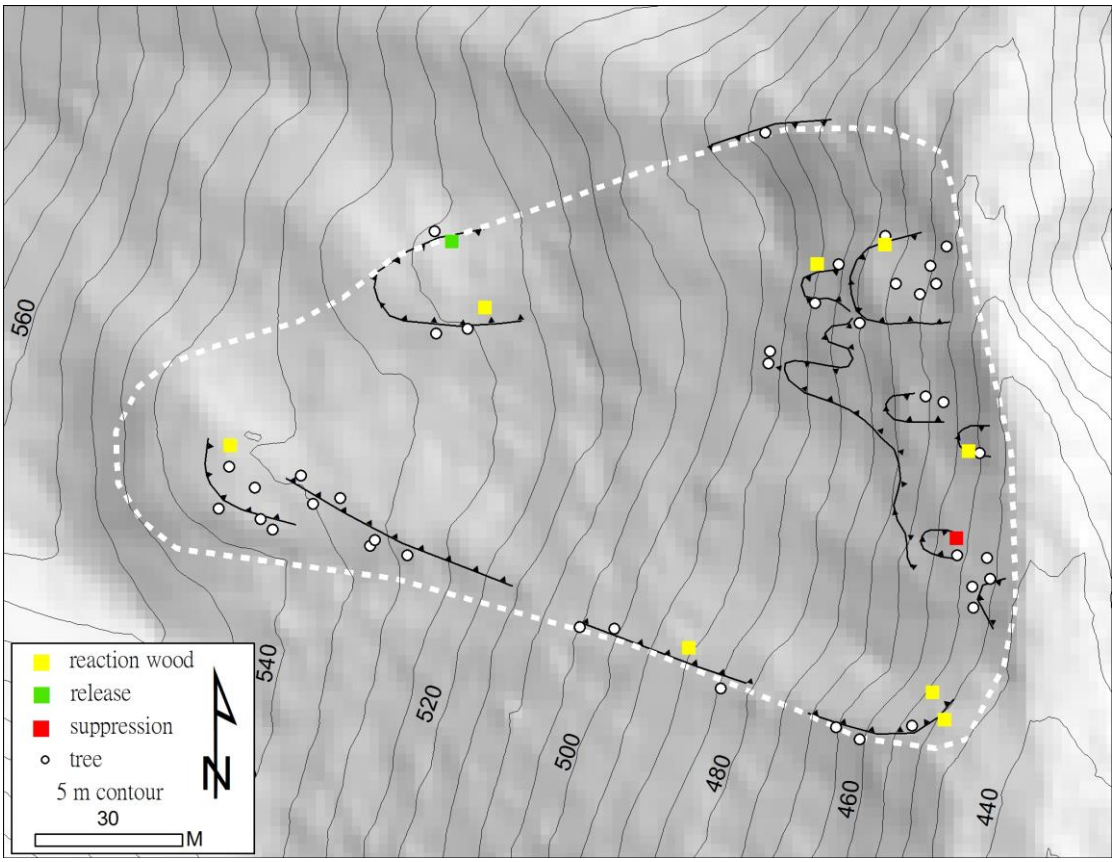

Figure 21 2009 growth disturbance location and type

4.4 Harvest effect on water input

Between 1948 to 2016, maximum annual one-day and thirty-day water input that results from fully harvested conditions is significantly greater than water input that results from fully forested conditions (paired t-test, signed-rank test, 95% confidence level). After 1990, maximum one-day precipitation coincidentally decreases. As a consequence, changes in water-input that might be due to harvest are not significant enough to increase maximum annual one-day and thirty-day water input above pre-1990 levels. (rank-sum test, 95% confidence level). Annual maximum series of one-day and thirty-day accumulated precipitation and water-input are plotted in Figures 22 and 23. In each figure, the 5, 10, 25 and 50 year events are indicated.

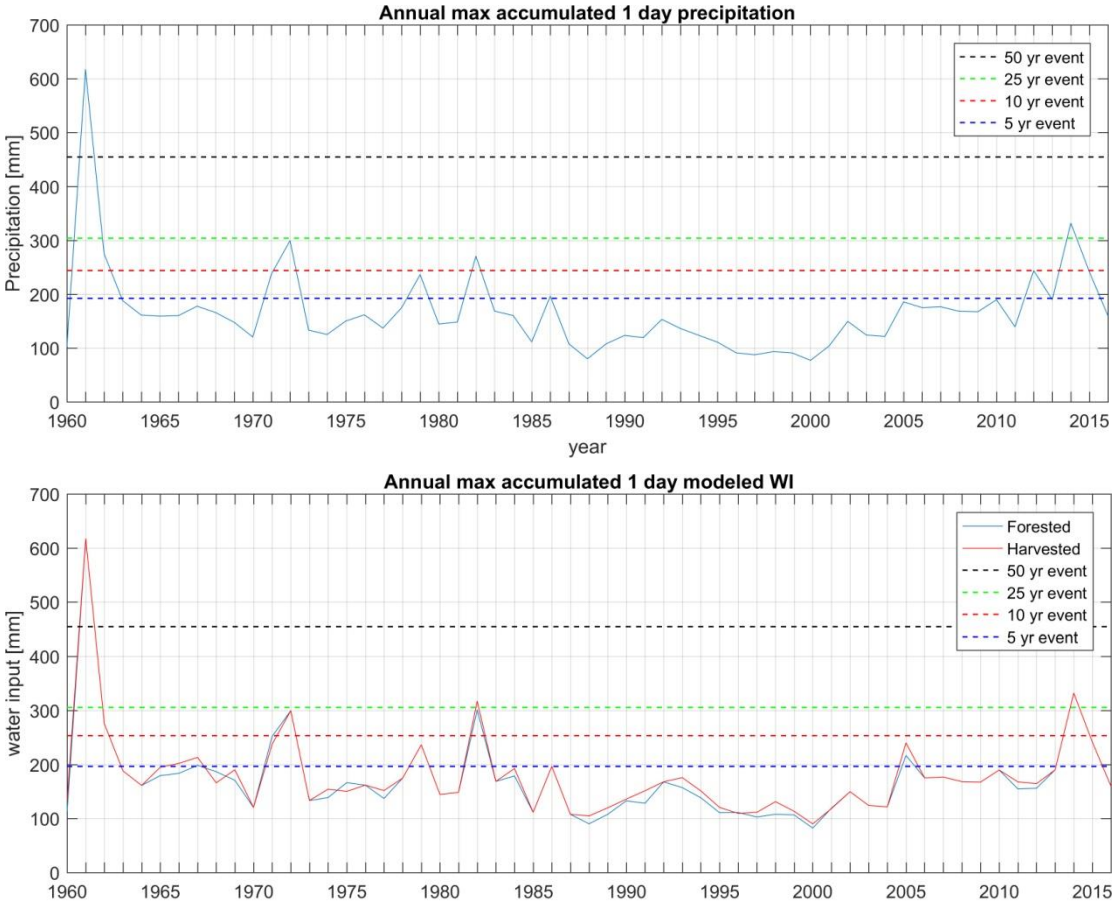

Figure 22 Annual time series of maximum one day accumulated rainfall and water input. Dashed lines indicate magnitude of different return period events.

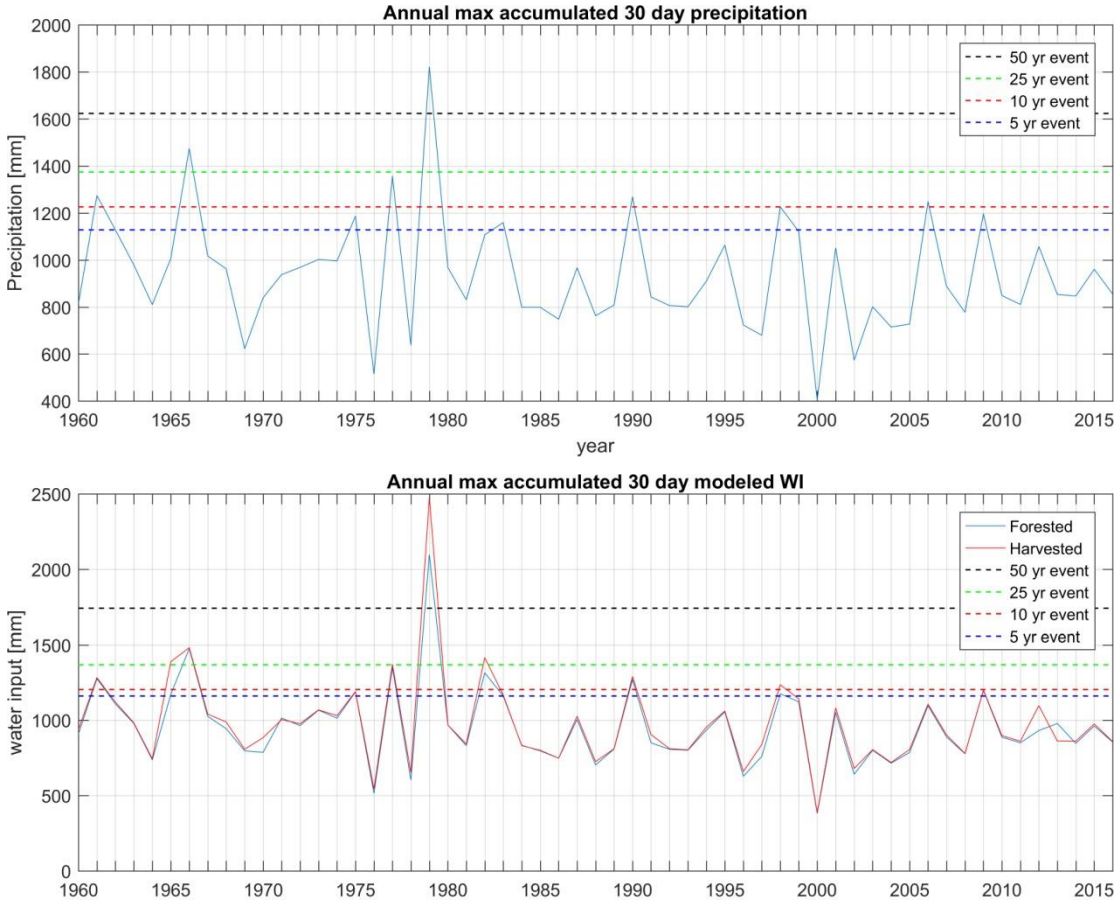

Figure 23 Annual time series of maximum thirty day accumulated rainfall and water input. Dashed lines indicate magnitude of different return period events.

4.5 Harvest effect on peak flows

Over the three year observation period, accumulated runoff from modeled, fully harvested conditions is 13% higher than accumulated runoff from modeled, fully forested conditions (Figure 24). Flow magnitude versus return period for maximum one day flows are shown in Figure 25. Return period in Figure 25 is computed from a partial duration series of the modeled hydrograph for fully forested conditions. Harvesting causes flow magnitudes of flows smaller than the 1.1 year flow event to increase. Flow magnitudes greater than a 1.1 year flow event are not increased.

The average increase in flow magnitude for four ranges of flow return periods are listed in Table 9. The 0 to 0.4 year flows and the 0.4 to 1 year return period flows are listed to permit comparison to Jones et al. (1996) and Beschta et al. (2000). The 1 to 2 year flow event range is listed because it bounds the recurrence interval of bank full stage or effective discharge in the Pacific Northwest (Castro and Jackson, 2001). All

other flows larger than a 2-year flow event are grouped in the last flow range. Fully harvested conditions causes flow magnitude of both the 0 to 0.4 year flows and the 0.4 to 1 year flows to increase more than 10%. The change in magnitude of the 1 to 2 year flows, and the 2 year and greater return period flows change (decrease) by only a few percent.

The annual maximum series of one-day and thirty-day accumulated flow are plotted in Figure 26. After harvest in 1990, maximum thirty-day accumulated flow is significantly higher than before harvest but maximum one-day accumulated flow is not significantly higher (two-sample t test and rank-sum test, 95% confidence). The increase in thirty-day accumulated runoff contrasts with trends in thirty-day water input and precipitation.

The water budget for fully forested conditions (determined by calibrating BGM output to the three years of observed flow) are listed in Table 10. The water budget for fully harvested conditions are also listed in Table 10. The runoff ratio (total runoff from the basin outlet divided by total precipitation input in the basin during the calibration period) increases from 0.76 to 0.86 after harvest. Annual evapotranspiration decreases by about 40% and the water that enters the soil increases by roughly 11%. Water budget metrics listed in Table 10 are described in Table 11

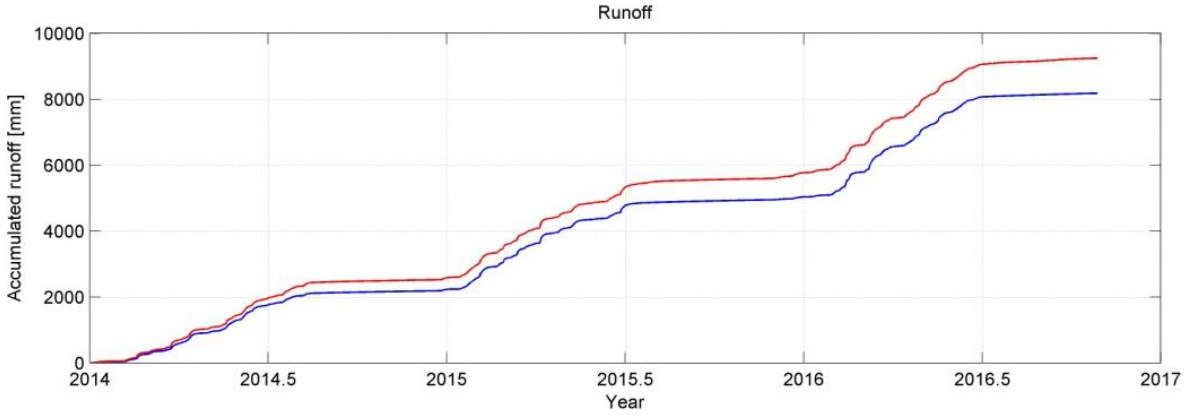

Figure 24 Fully cleared conditions causes a 13% increase in accumulated runoff over three year observation period

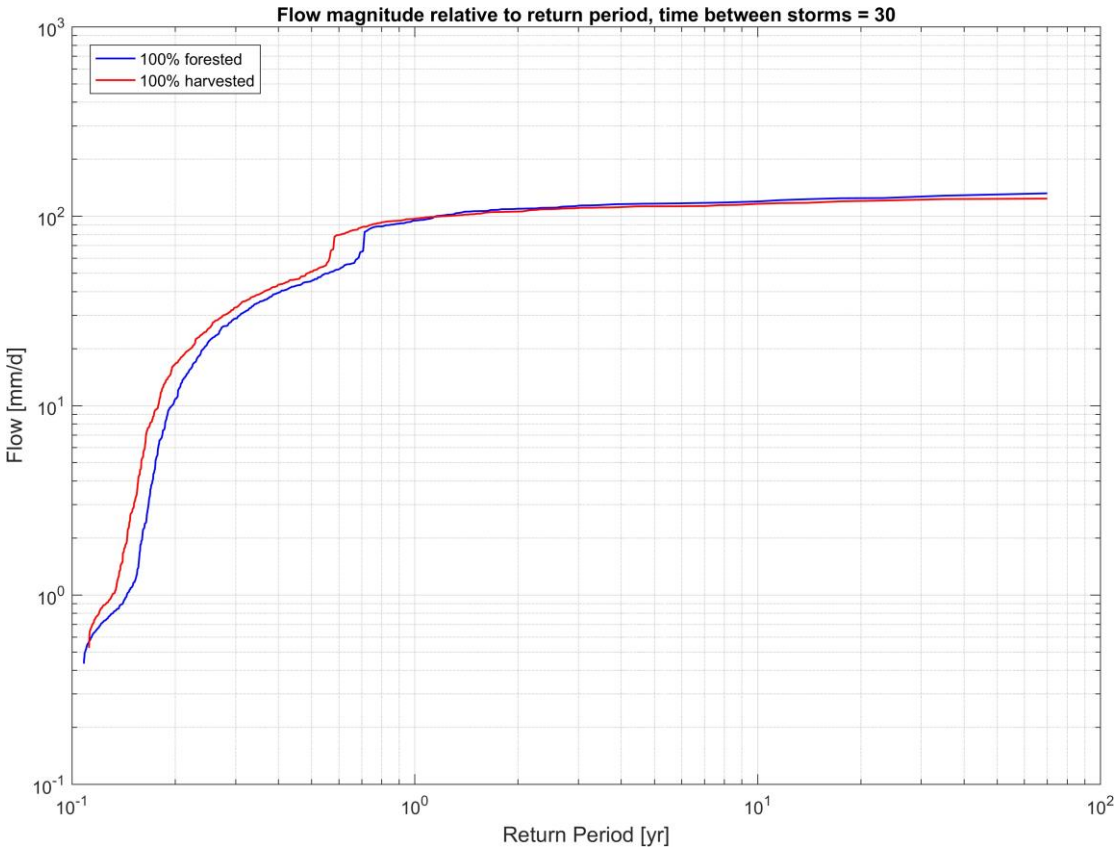

Figure 25 Flow magnitude relative to return period for forested and harvested parameter sets. Return period is computed from a partial duration series of the modeled hydrograph.

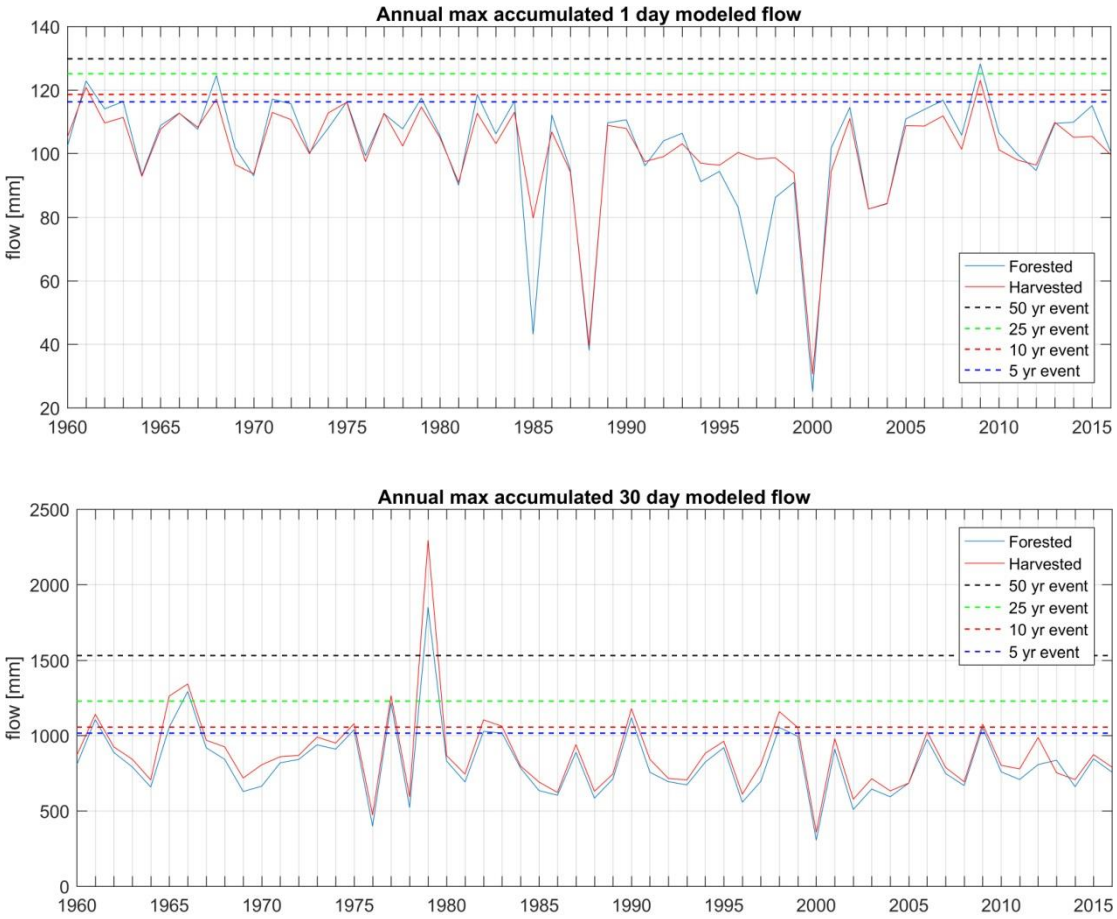

Figure 26 Plot of maximum one-day and thirty-day accumulated flow for fully forested and harvested conditions. Following harvest, the increase in maximum one day flow is insignificant but the increase in maximum thirty day flow is significant.

Table 9 Percent change in peak flow for four ranges of flow return period

Return Period [yrs]	<0.4	0.4-1	1-2	>2
Peak flow [%]	17	14	-2	-4

Table 10 Summary of modeled water budget for forested and harvested conditions

Metric	Fully forested conditions	Fully harvested conditions,
Drainage ratio	0.70	0.77
Interception ratio	0.07	0.0002
Evapotranspiration ratio	0.23	0.13
Runoff ratio, observed	0.76	0.76
Runoff ratio, modeled	0.76	0.86
Surface runoff ratio	0.07	0.085
Subsurface ratio	0.84	0.83

Ground water ratio	0.09	0.08

Table 11 Description of water budget metrics

Metric	Description*
Drainage ratio	Accumulated runoff divided by accumulated water input
Interception ratio	Accumulated interception divided by accumulated water input
Evapotranspiration ratio	Accumulated evapotranspiration divided by accumulated water input
Runoff ratio, observed	Accumulated observed runoff divided by accumulated water input
Runoff ratio, modeled	Accumulated modeled runoff divided by accumulated water input
Surface runoff ratio	Accumulated surface runoff divided by accumulated runoff at basin outlet
Subsurface flow ratio	Accumulated subsurface flow divided by accumulated runoff at basin outlet
Groundwater flow ratio	Accumulated groundwater flow divided by accumulated runoff at basin outlet

*Note: Accumulated over the period used to calibrate BGM: 2013 to 2016

4.6 Landslide sensitivity to scour and pore water pressure

4.6.1 Conceptual model 1

In conceptual model one, the water table and landslide are controlled by a single fixed surface of rupture. FS is reduced 0.1 for every 10 meter increase of hydraulic head. In contrast, 10 meters of scour into the toe reduces FS by only 0.01 to 0.02. For the high strength parameter set, the water table needs to have a depth of at least 20 meters before the FS drops below 1. More than 25 meters of scour into the toe is needed to drop the FS below 1. For the low strength parameter set, a water table of 8 meters causes the FS to drop below 1 and 25 meters of scour into the toe cause FS to drop below 1. Under both strength scenarios, if the water table is sufficiently high, only a few meters of scour into the toe causes FS to drop below 1 (Figure 26).

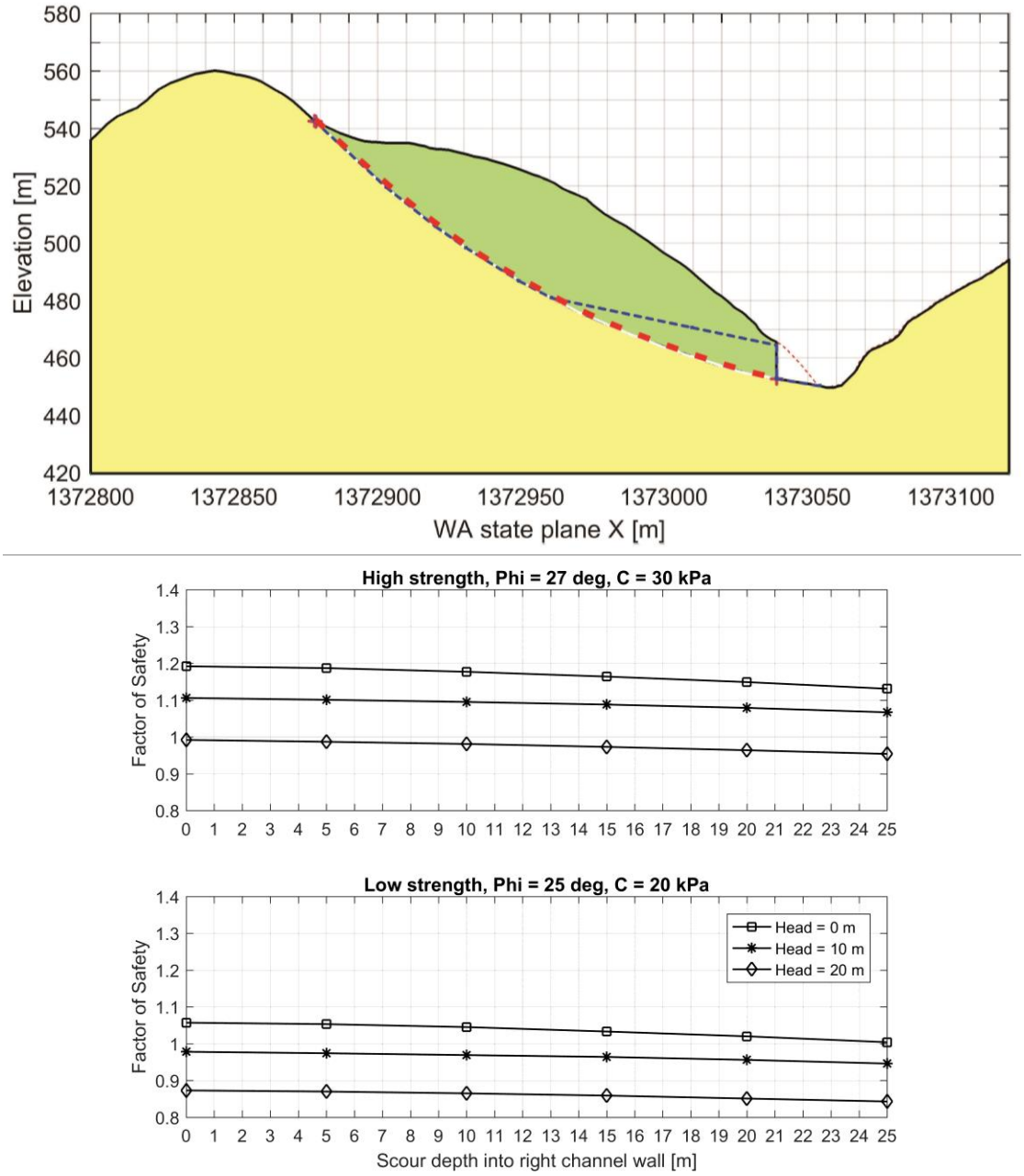

Figure 27 Conceptual model 1 - Factor of Safety as a function of lateral scour for three soil water scenarios. Dashed blue line is water table, dashed red line is surface of rupture. Boundary between green and yellow regions is impermeable surface that controls water table height.

4.6.2 Conceptual model 2

In conceptual model 2, the water table is controlled by an impermeable boundary located below the surface of rupture. When the water table is located below the surface of rupture, changes in hydraulic head have no effect on the stability of the landslide; only lateral scour into the toe reduces FS. Once the water table is above the surface of rupture, FS is reduced 0.8 to 0.9 for every 10 m of hydraulic head. In contrast, 10 meters of lateral scour cause a 0.04 to 0.06 reduction of FS. The landslide in conceptual model 2 is four to six times more sensitive to lateral scour into the toe and slightly less sensitive to hydraulic head than the landslide in conceptual model 1. (Figure 28)

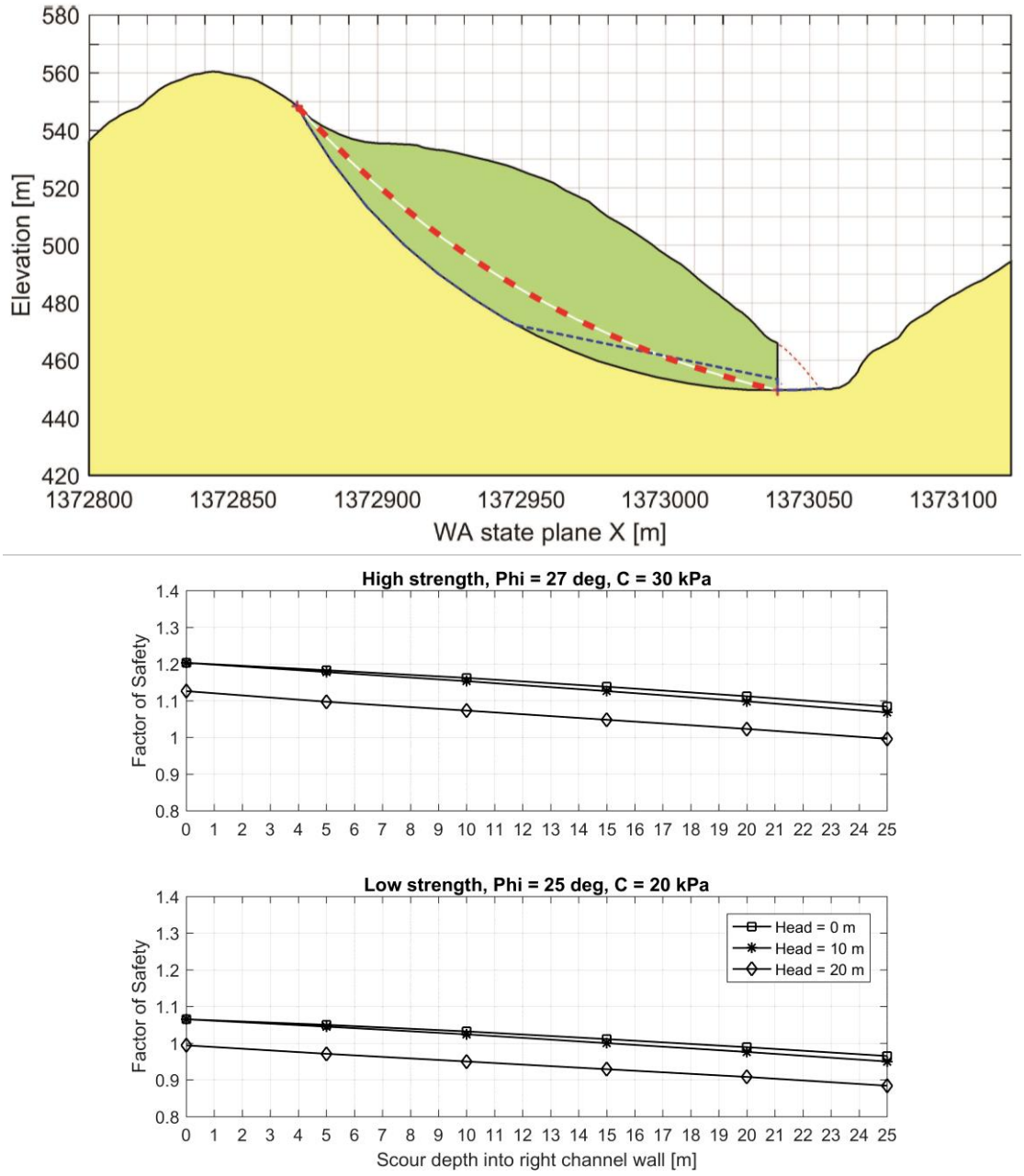

Figure 28 Conceptual Model 2 - Factor of Safety as a function of lateral scour for three soil water scenarios. Dashed blue line is water table, dashed red line is surface of rupture. Boundary between green and yellow regions is impermeable surface that controls water table height.

5. Discussion

5.1 Possible landslide activity triggers

5.1.1 Pore water pressure

Dendrogeomorphic reconstruction of the landslide activity record indicates that the

deep-seated landslide may have moved in 1998 to 1999, 2003 to 2004 and 2009. Deep-seated landslides are known to mobilize following heavy antecedent precipitation (Iverson and Major, 1987; GEER, 2014;). If pore water pressure is controlling the timing of deep-seated activity, it stands to reason that large magnitude thirty-day accumulated water input (rainfall plus snowmelt) events might coincide with all years of activity.

Examination of the water input record relative to the deep-seated landslide activity record reveals that only the 1998 to 1999 and 2009 landslide events coincide with a large thirty-day accumulated water input event. The absence of a large thirty-day accumulated water input event in 2003 to 2004 substantiates the notion that landslide stability may be sensitive to other triggers such as scour. While neither conceptual model can be unquestionably accepted as being representative of subsurface conditions, landslide activity during years of low antecedent water input and the possible sensitivity of the landslide to scour does lend to the argument that Conceptual Model 2 may be an approximation of subsurface conditions. With regard to scour, the question remaining is what controls it: debris flows or high peak flows?

5.1.2 Scour into the landslide toe

Of the three landslide activity years, modeled one-day accumulated peak flow is less than a 10-year flow event for all years except 2009. In 2009, as a consequence of rain on snow effects, peak flows are exceptionally high and are nearly equal to a 25-year event. It is possible that this large flow event in 2009 caused scour along the landslide toe.

On the other hand, debris flows likely occurred during all years of deep seated landslide activity. Because periods of deep seated landslide activity consistently coincide with years of debris flows, it's plausible that a debris flow caused the 2009 landslide event and that in general, debris flow scour may be the dominant landslide trigger.

Comparison of the basal shear stress caused by a 25-year flood to the basal shear stress caused by a debris flow helps frame the role each process may have had in scouring the toe of the landslide in 2009. In the channel at the toe of the deep-seated landslide, alders growing along the channel wall that are older than the 2009 debris flow event are approximately 2.5 meters above the channel bed. Assuming a flow depth of 2.5 meters and using a reach average slope, basal shear stress can be approximated using:

$$\tau = \rho g h \sin\theta \qquad \text{E.3}$$

Where τ is the reach average basal shear stress, ρ is density, g is acceleration due to gravity, h is flow depth and θ is the reach average slope angle of the channel.

If differences in flood and debris flow depth are ignored, simply because of the difference in density, shear stress along the base of the debris flow is nearly twice as high as the flow of water (assuming a debris flow density of 2000 kg/m^3, Costa and Fleisher, 1984). If differences in depth are considered, the difference in basal shear stress is much larger. Flow depth estimated using Manning's Formula for a 25-year peak flow event and the channel geometry, slope and roughness at the toe of the landslide is only 0.5 meters. A depth of 0.5 meters results in a reach-average basal shear stress that is nearly a magnitude less than the debris flow. The large difference in basal shear stress between the 25-year flood and a debris flow supports the notion that a debris flow is more likely to have controlled scour rates into landslide toe in 2009.

5.2 Timber harvest effect on the possible landslide triggers

Despite several lines of evidence that support the hypothesis that debris flows control the timing of deep-seated landslide activity, the fact that all three possible landslide triggers coincide with at least one period of landslide activity makes it difficult to simply rule out any one processes. Because the ultimate goal of this study is to determine how harvesting on and upstream of the landslide affected landslide stability, possible harvest effects on all three process are discussed below.

5.2.1 Timber harvest effect on water input

Paired t-test analysis demonstrates that water input under fully harvested conditions is significantly higher than that from fully forested conditions, a finding that matches modeled observations in the Pacific Northwest (Marks et al., 1996); Also, based on the modeled water budget (Table 10), evapotranspiration decreases by about 40% and water that enters the soil increases by roughly 11%.

The comparison of fully forested to fully harvested conditions in this study assumes that under fully harvested conditions, trees are permanently removed from the basin. In reality, all harvests in the basin were promptly planted to establish a tree farm and as trees grow, the hydrologic setting associated with the harvested condition gradually returns to a forest-like hydrologic setting. For example, evapotranspiration rates of a harvested conifer plantation required only 12 years to return to pre-harvest rates on Vancouver Island (Jassal et al., 2009). Consequently, the results of this study really only provide a sense how water input was affected during the first few years following the harvest.

On the landslide in East Fork Kunamaskt Creek, the trees were harvested in 1981 and planted by 1982 (WA DNR). By 1998 and 2009 the plantation would have been over 16 and 27 years old respectively. Therefore, by the time of landslide activity, the amount of water stored in the landslide may have been only slightly higher than or equal to that expected under fully forested conditions and the harvest would have had little effect on pore water pressures. If landslide activity was triggered by pore water pressure, the activity would have occurred under fully forested conditions too.

5.2.2 Timber harvest effect on peak flows

Model results demonstrate that harvests cause the magnitude of 1.1-year or smaller events to increase but flow events that have a magnitude larger than 1.1-year event may not be affected. Moreover, paired t-test analysis of maximum annual 1-day peak flows from harvested and forested basins shows that there may not be a significant difference in the mean value. Paired watershed studies in Oregon have found harvest to have an effect on peak flows that have a magnitude equal to or smaller than the 0.4 to 10 year event (Harr 1986, Jones and Grant, 1996, Beschta et al., 2000, Grant et al., 2008). Although the maximum return period of peak flows affected by timber harvest determined in this study is on the low end of reported values, the finding that only the lower return period flows are affected by harvesting is consistent with the other studies. Because the flow event that occurs in 2009 is a 25-year event and the magnitude of the event far exceeds the range of flows determined in this study or observed in other studies to be influenced by harvest, the harvest likely had little effect on the magnitude of the 2009 flow. If landslide activity was triggered by peak flow caused channel scour, the activity likely would have occurred regardless of vegetation conditions in the headwaters of the basin.

5.2.3 Timber harvest effects on debris flows

Debris flows can be initiated from the mobilization of landslide debris or channel deposits. The frequency of shallow landslides is known to increase following timber harvest (Sidle, 1992, Montgomery et al., 2000) and Rengers et al. (2016) found that present day tree density as well as precipitation exert a strong control on the location of debris flow initiation in Colorado drainages. At East Fork Kunamaskt creek, an increase in debris flow activity following tree harvest was observed in the headwaters. Most debris flows initiated from landslides along the channel wall.

East Fork Kunamaskt Creek is located in a setting of rapid uplift countered by rapid erosion. Debris flows and landslides occur naturally. It’s plausible that the sudden increase in debris flow events after 1990 was a natural phenomenon that would have

occurred regardless of harvest history; however, two sample t-test and rank-sum tests results show that mean 1-day and 30-day accumulated rainfall and water-input do not increase during the period of frequent debris flows. In fact, 1-day accumulated rainfall and water input is significantly lower during the period of frequent debris flows.

The absence of above average 1-day and 30-day precipitation during the period of increased debris flow frequency suggests the timing of increased debris flows after tree harvest was caused by the removal of trees from the landscape. Unlike evapotranspiration rates, effective cohesion takes 15 to 25 years to redevelop follow harvest if replanting is successful and possibly over a century if replanting is not successful (Schmidt et al., 2001). All of the debris flow events occur during the possible period of reduced effective cohesion and therefore may have been caused by the 1990 tree harvests. By triggering debris flows that flowed past the toe of the landslide, timber harvest may have indirectly triggered deep seated landslide activity within the basin.

5.3 Mitigating tree harvest caused fluvial effects on downstream landslides

Findings in this study support the notion that upstream tree harvests affected a down-stream, deep-seated landslide in East Fork Kunamaskt Creek by triggering debris flows that flowed past and debuttressed the landslide; however, the susceptibility of the landslide to debris flow caused scour is largely because of the channel location of the tree harvests relative to the channel location of the deep-seated landslide: tree harvests occurred in the hollow or debris flow source zone of the channel and the landslide constricts the cascade reach or scour zone of the channel. If the landslide were located in a pool-riffle reach or deposition zone of the channel, beyond the runout distance of a potential debris flow, debris flows likely would not have passed the toe of the landslide. In other words, debris flows triggered by upstream harvests would not have affected the landslide.

Future harvests can avoid triggering similar deep-seated landslide processes by determining what channel reach the harvest encompasses. If a proposed harvest is taking place in the source zone of a channel such as a hollow or a colluvium reach, the channel downstream of the harvest should be examined for the presence of a landslide that is constricting the scour reach of the channel. If a landslide is found within the scour reach of the channel, and if the source zone of the channel is not already excluded from the harvest, the hollow or colluvium reaches of the channel should be specifically protected to prevent debris flows and subsequent debuttressing of the down-stream landslide. If a deep-seated landslide is found in the deposition zone of the channel, beyond the runout distance of a possible debris flow from the proposed timber harvest, changes to the harvest plan aimed at minimizing fluvial effects to the

downstream landslide are not needed.

6. Conclusion

Three periods of landslide activity are identified from a dendrogeomorphic study of an existing deep-seated landslide located in the East Fork Kunamaskt Creek watershed on the west side of the Olympic Mountains. Because the deep-seated landslide constricts the channel in the debris flow scour zone, it is susceptible to scour and debuttressing. By comparing the periods of landslide activity to modeled water input (rainfall plus snowmelt), modeled stream flow, debris flow records and tree harvest records, and incorporating the results of a slope stability sensitivity analysis, possible landslide triggers are inferred.

Slope stability analysis of the landslide demonstrates that the landslide can be destabilized by both scour and pore water pressure. Depending on the location of the surface of rupture and the impermeable layer that controls the height of the water table, the landslide may be more sensitive to scour. Large water input and stream flow events coincide with periods of landslide activity but occur after timber harvest is expected to have an effect. In contrast, debris flows coincide with each year of landslide activity and debris flow frequency dramatically increases following harvest of the headwaters during the period that effective cohesion is expected to be reduced as a result of tree harvests. Moreover, during the period of increased debris flow frequency, there is no significant increase in annual maximum 1-day or 30-day accumulated precipitation. It is therefore concluded that harvesting the headwaters triggered both debris flows in the headwaters and deep-seated landslide activity within the basin.

7. References

Alestalo, J., 1971, Dendrochronological interpretation of geomorphic processes: Fennia, v. 105, p. 1-139.

Anderson, E.A., 1976, A point energy and mass balance model of a snow cover: NOAA Technical Report NWS 19, 172 p.

Anderson, E.A., 2006, Snow accumulation and ablation model – Snow-17: http://www.nws.noaa.gov/oh/hrl/nwsrfs/users_manual/part2/_pdf/22snow17.pdf (accessed July , 2016).

Badger, T.C., 2007, Geologic assessment and mitigation alternatives: Bogachiel

Landslide, U.S. 101, XL-2953, Vicinity Mile Post 184.10 to 184.65, Jefferson County, Washington: Washington Department of Transportation, Olympia WA.

Batt, G.E., Brandon, M.T., Farley, K.A., Roden-Tice M., 2001, Tectonic synthesis of the Olympic Mountains segment of the Cascadia wedge, using two-dimensional thermal and kinematic modeling of therrnochronological ages: Journal of Geophysical Research, v. 106, n. B11, p. 26731-26746.

Beschta, R.L., Pyles, M.R., Skaugset, A.E., Surfleet, C.G., 2000, Peakflow responses to forest practices in the western cascades of Oregon, USA: Journal of Hydrology, v. 233, p. 102-120.

Benda L., Veldhuisen, C., Miller, D., Miller, L.R., 1998, Slope instability and forest land managers: A primer field guide: Earth Systems Institute, http://citeseerx.ist.psu.edu/viewdoc/download;jsessionid=7FEF1D145F10081ECB8019761F349B6A?doi=10.1.1.652.6684&rep=rep1&type=pdf, (accessed January 2017).

Brandon, M.T., Roden-Tice, M.K., Garver J.L., 1998, Late Cenozoic exhumation of the Cascadia accretionary wedge in the Olympic Mountains, northwest Washington State: GSA Bulletin, v. 110, n. 8, p.985-1009.

Chung, M-C., Tan, C-H., Chen, C-H., 2017, Local rainfall thresholds for forecasting landslide occurrence: Taipingshan landslide triggered by Typhoon Saola: Landslides, v. 14, p. 19-33.

Costa, J.E., and Fleisher, P.J., eds., 1984, Developments and Applications of Geomorphology, Berlin Heidelberg, Springer-Verlag.

Cruden, D.M., and Varnes, D.J., 1996, Landslide Types and Processes, Special Report , Transportation Research Board, National Academy of Sciences, v. 247, p. 36-75

Czajkowski, J.L., Bowman, J.D., 2014, Faults and earthquakes in Washington State: Washington Department of Natural Resources, 1 sheet.

Gerstel, W.J., and Lingley, W.S., 2000, Geologic Map of the Forks 1:100,000 Quadrangle, Washington: Washington State Department of Natural Resources, Olympia, 2 sheets, 42 p. text.

Fritts, H.C., 1976, Tree Rings and Climate: New York and San Francisco, Academic Press.

GEO-SLOPE International Ltd., 2015, Stability Modeling with SLOPE/W, http://downloads.geo-slope.com/geostudioresources/8/0/9/books/slope%20modeling.pdf?v=8.0.10.6, (accessed December 2016).

Geotechnical Extreme Events Reconnaissance, 2014, The 22 March 2014 Oso Landslide, Snohomish County, Washington: https://snohomishcountywa.gov/DocumentCenter/View/18180 (accessed June 2016)

Grant, G.E., Lewis, S.L., Swanson, F.J., Cissel, J.H., McDonnell, J.J., 2008, Effects of forest practices on peak flows and consequent channel response: A state-of-science report for western Oregon and Washington: United States Department of Agriculuture, Forest Service, General Technical Report PNW-GTR-760.

Guthrie, R.H., 2002, The effects of logging on frequency and distribution of landslides in three watersheds on Vancouver Island, British Columbia: Geomorphology, v. 43, p. 273-292.

Harr, R.D., 1977, Water flux in soil and subsoil on a steep forested slope: Journal of Hydrology, v. 33, p. 37-58.

Harr, R.D., 1986, Effects of clearcutting on rain-on-snow runoff in western Oregon: A new look at old studies: Water Resources Research, v. 22, n. 7, p. 1095-1100.

Hungr, O., Leroueil, S., Picarelli, L., 2014, Varnes classification of landslide types, an update: Landslides, v. 11, p. 167-194

Istanbullouglu, E., Wang, T., Wedin, D.A., 2012, Evaluation of ecohydrologic model parsimony at local and regional scales in a semiarid grassland ecosystem: Ecohydrology, v. 5, p. 121-142.

Iverson, R.M., and Major, J.J., 1987, Rainfall, ground-water flow, and seasonal movement at Minor Creek landslide, northwestern California: Physical interpretation of empirical relations: Geological Society of America Bulletin, n4, p. 579-594.

Iverson, R.M., 2000, Landslide triggering by rain infiltration: Water Resources Research, v. 36, n.7, p. 1897-1910.

Jassal, R.S., Black, T.A., Spittlehouse, D.L., Brummer, C., Nesic, Z., 2009, Evapotranspiration and water use efficiency in different-aged Pacific Northwest Douglas-fir stands: Agricultural and Forest Meteorology, v. 149, p. 1168-1178.

Johnson, A.C., Edwards, R.T., Erhardt, R., 2007, Ground-water response to forest harvest, implications for hillslope stability: Journal of American Water Resources Association, v. 43, n.1.

Jones, J.A., and Grant, G.E., 1996, Peak flow responses to clear-cutting and roads in small and large basins, western Cascades, Oregon: Water Resources Research, v. 32, p. 959-974.

Keck, J., Hsiao, C-Y., Lin, B-S., Chan H-M., Wright, W., 2014, Spatiotemporal landslide activity derived from tree-rings: the Tieliku Mingsui landslide, northern Taiwan: Journal of Chinese Soil and Water Conservation, v. 45(1), p. 36-48.

Keim R.F., Skaugset A.E., 2003, Modeling effects of forest canopies on slope stability: Hydrological Processes, v.17, p. 1457-1467.

Laio, F., Porporato, A., Ridolfi, L., Rodriguez-Iturbe, I., 2001, Plants in water controlled ecosystems: Active role in hydrologic processes and response to water stress II. Probabilistic soil moisture dynamics: Advances in Water Resources v. 24, p.707–723.

Lopez-Saez, J., Corona, C., Stoffel, M., Schoenieich, P., Frederic Berger, F., 2012, Probability maps of landslide reactivation derived from tree-ring records: Pra Bellon landslide, southern French Alps: Geomorphology, v. 138, p. 189-202

Marks., D., Kimball, J., Tingey, D., Link, T., 1998, The sensitivity of snowmelt processes to climate conditions and forest cover during rain-on-snow: a case study of the 1996 pacific Northwest flood: Hydrological Processes, v. 12, p. 1569-1587.

Martin, Y., Rood, K., Schwab, J.W., Church, M., 2002. Sediment transfer by shallow landsliding in the Queen Charlotte Islands, British Columbia. Canadian Journal of Earth Sciences, v. 39, p.189–205

Miller, D. J., 1995, Coupling GIS with physical models to assess deep-seated

landslide hazards: Environmental & Engineering Geoscience, v. 1, p. 263-276.

Miller, D. J., and J. Sias. 1998. Deciphering large landslides: linking hydrological, groundwater and slope stability models through GIS: Hydrological Processes, v. 12, p. 923- 941.

Montgomery, D.R., and Buffington, J.M., 1997, Channel-reach morphology in mountain drainage basins: GSA Bulletin, v. 109, n. 5, p. 596-611.

Montgomery, D.R., Schmidt, K.M., Greenberg, H.M, Dietrich, W.E., 2000, Forest clearing and regional landsliding: Geology, v. 28, n. 4, p. 311-314

National Weather Service River Forecast System User Manual Documentation: Office of Hydrologic Development: http://www.nws.noaa.gov/ohd/hrl/nwsrfs/users_manual/htm/xrfsdocpdf.php, (accessed July 2016).

,

Nathan, R.J., McMahon, T.A., 1990, Evaluation of automated techniques for base flow recession analysis: Water Resources Research, v. 26, n. 7, p. 1465-1473.

Natural Resources Conservation Service: https://www.nrcs.usda.gov/wps/portal/nrcs/, accessed July, 2016).

Orr, E.I., and Orr, W.N., 1996, Geology of the Pacific Northwest: New York, McGraw Hill Companies, 337 p.

Pazzaglia F.J., and Brandon M.T., 2001, A fluvial record of long-term steady-state uplift and erosion across the Cascadia Forearc High, Western Washington State: American Journal of Science, v. 301, p. 385-431.

PRISM Climate Group, Northwest Alliance for Computational Science and Engineering, http://prism.oregonstate.edu/ (accessed July, 2016).

Puget Sound Lidar Consortium, 2016, http://pugetsounlidar.ess.washington.edu/About_PSLC.htm (accessed January, 2016)

Pyles M.R., Mills, K., Saunders, G., Mechanics and stability of the Lookout Creek Earth Flow: Bulletin of the Association of Engineering Geologists, v. 24, n. 2, p.

267-280.

Raleigh M.S., and Lundquist J.D., 2012, Comparing and combining SWE estimates from the SNOW-17 model using PRISM and SWE reconstruction: Water Resources Research, v. 48, W01506

Rantz, S.E., 1982, Measurement and Computation of Streamflow: Volume 2. Computation of Discharge: United State Department of the Interior, Geological Survey Water-Supply Paper 2175, https://pubs.usgs.gov/wsp/wsp2175/pdf/chapter10_vol2.pdf (accessed July, 2016).

Rengers, F.K., McGuire L.A., Coe, J.A., Kean, J.W., Baum, R.L, Staley, D.M., Godt, J.W., 2016, The influence of vegetation on debris-flow initiation during extreme rainfall in the northern Colorado Front Range: Geology, v. 44, p. 823-826.

Robinson, L., Newell, J.P., Marzluff, J.M., 2005, Twenty-five years of sprawl in the Seattle region: growth management responses and implications for conservation: Landscape and Urban Planning, v. 71, p. 51-72

Schmidt, K.M., Roering, J.J., Stock, J.D., Dietrich, W.E., Montgomery, D.R., and Schaub, T., 2001, The variability of root cohesion as an influence on shallow landslide susceptibility in the Oregon Coast Range: Canadian Geotechnical Journal, v. 38, p. 995-1024.

Schroder, J.F., 1978, Dendrogeomorphological analysis of mass movement on table cliffs plateau, Utah: Quaternary Research, v. 9, p.168-185.

Shinker, J.J., ande Bartlein, P.J., 2009, Spatial Variations of effective moisture in the western United States: Geophysical Research Letters, v. 37, L02701.

Sidle, R.C., 1992, A theoretical model of the effect of timber harvesting on slope stability: Water Resources Research, v. 28(7), p. 1897-1910.

Silhan, K. 2016, How different are the results acquired from mathematical and subjective methods in dendrogeomorpholoy? Insights from landslide movements: Geomorphology, v. 253, p. 189-198.

Skaugset, AE., 1997, Modeling root reinforcement in shallow forest soils [PhD thesis]:

Corvallis, Oregon State University, 300 p.

Stoffel, M., Bollschweiler, M., Butler, D., and Luckman, B., 2010, Tree Rings and Natural Hazards: Springer, New York.

Swanson, F.J., Swanston D.N., 1977, Complex mass-movement terrains in the western Cascade Range: Geological Society of American, Reviews in Engineering Geology, v. 3.

Washington State Department of Natural Resources, http://www.dnr.wa.gov/geologyportal (accessed January , 2016).

Wegmann, W.K, and Pazzaglia, F.J., 2002, Holocene strath terraces, climate change, and active tectonics: The Clearwater River basin, Olympic Peninsula, Washington State, GSA Bulletin, v. 114, n. 6, p. 731-744.

Wemple, B.C., Swanson, F.J., Jones, J.A, 2001, Forest roads and geomorphic process interactions, Cascade Range, Oregon: Earth Surfaces Processes and Landforms, v. 26, p. 191-204.

Wolter, A., Ward, B., Millard, T., 2010, Instability in eight sub-basins of the Chilliwack River Valley, British Columbia Canada: A comparison of natural and logging-related landslides: Geomorphology, v. 120, p. 123-132.

Western Regional Climate Center, http://www.wrcc.dri.edu/summary/climsmwa.html, (accessed January 2016).

Wyllie, D.C., and Mah, C.W., 2005, Rock slope engineering: civil and mining, 4th edition: London and New York, Spon Press, 431 p.